ATMOSPHERIC, OCEANIC
AND PLANETARY PHYSICS
UNIVERSITY OF OXFORD

DPhil First Year Report

Dynamics and circulation of Venus and Titan

João Manuel Mendonça

Supervisor
Prof. Peter L. Read

Co-Supervisor
Dr. Stephen R. Lewis
(The Open University)

August 2009

E-mail: Mendonca@atm.ox.ac.uk

Dynamics and Circulation of Venus and Titan

Abstract:

The main objective of my DPhil is to study and understand the atmospheric circulation of slowly rotating "planets" such as Venus and Titan, that despite their differences, exhibit a strong planetwide super-rotating zonal winds and other similar features in their atmospheres.

To achieve this goal, we use Simplified General Circulation Models (SGCMs) adapted for both atmospheres. These models use simplified parameterisations as explained in Chapter 4, 6 and 7. These simplifications save computational time and avoid difficulties regarding the observational data about these astronomical objects, nevertheless they attempt to keep a realistic dynamic circulation of the atmosphere, essential for our objectives.

In the first year of my PhD project, I started by reading the literature on the subject of General Circulation Models (GCMs) for Venus and Titan, with special emphasis on simplified models and methods to extend the SGCM for Venus improving the radiative scheme. The new parameterisation of the radiative scheme in the SGCM for Venus, transforms the model to a more complete version (Full GCM) which allows us to better compare the results of the model with observational data. Amongst other features, the possible existence of a transport barrier in the atmosphere of Venus from the analysis of potential vorticity (PV) fields, and the possible influence of eddy momentum fluxes in the middle atmosphere near the jets, were investigated. The basis for the first Simplified General Circulation Model (SGCM) for Titan was developed, and has a similar structure than the one for Venus.

This report is a description of the work done, and is structured as follows: I first write a literature review, followed by the results of the research I have done for each Astronomical object (Venus and Titan), and finally present a summary of my future plan of work.

Contents

List of Figures

List of Tables

CHAPTER 1

Introduction

Contents

1.1 Super-rotating Atmospheres of Venus and Titan

The circulation of the atmospheres of both Venus and Titan are well known to exhibit strong super-rotation and a variety of similar enigmatic features, but both remain poorly understood (see Chapter 2). The super-rotation is characterised by a faster rotation of the atmosphere compared to the rotation rate of the solid body, and is most likely found in slowly rotating "telluric bodies". This is a surprising phenomenon because it is counter intuitive if we think on results of solid bodies in a regime of no rotation. Having a better understanding of the mechanism of formation and maintenance of this phenomenon, we can draw a more accurate theory about the global circulation of both atmospheres.

When studying the circulation of Venus and Titan's atmospheres, some general questions arise about their super-rotation:

- What is the mechanism that drives these slow rotating "planets" to an atmospheric super-rotation?
- Is the super-rotation an inevitable state of slow rotating "planets"?
- What are the atmospheric and slow body's parameters for which the atmosphere is sensitive to in its transition to super-rotation?
- Are the phenomena such as the polar vortex or the large-scale wave patterns observed in the atmosphere of Venus, common in the super-rotating atmospheres?

This DPhil investigates mainly the atmospheric circulation of two "worlds": Venus and Titan. Despite the differences in the physical body, different rates of vertical and horizontal profiles for heating and cooling (Venus: important diurnal variations; Titan: important seasonal variations) and the amount of total atmospheric mass, both rotate slowly and have a very efficient way of retaining IR radiation in the atmosphere, which increases the vertical static stability of the atmosphere. Here we investigate the mechanism and the consequences

in the dynamics of the atmosphere produced by the atmospheric circulations in these two "planets".

The aim of the comparative study about both atmospheres is to understand a variety of atmospheric phenomena governed by common physical laws. Understand why Titan and Venus atmospheric's circulation produce similar phenomena, could help to answer some key scientific questions about the atmospheric super-rotation, that will be explored in my PhD project:

- Which types of waves are most important for sustaining super-rotation? - Planetary waves, Gravity waves or Thermal tides?
- What is the role of topography and surface interactions?
- What is the role of seasonal variations? - Much larger on Titan than on Venus.
- What is the dynamic role of clouds either as passive or active factors? Also what determines distribution and properties of clouds across the planet? The model used in this work (Lee et al., 2009), obtains a cloud distribution similar to observations.

1.2 Proposed Methodology

An essential tool used in my DPhil project is a numerical simulation of the atmospheric circulation with General Circulation Models (GCMs). These models have been very important in investigating the climate and weather forecasting on Earth as well. Changing the general parameters that characterise the planets, it is possible to adapt the model which solves the primitive equations using for example a discretisized finite difference scheme (the one used in our project). It is possible to modify the physical parameterisation as well, to better adapt the planet atmosphere in study and solve problems regarding time spent in computation. The dynamical part of the GCM usually remains the same due to the universal laws of fluids in the atmosphere, but can be modified, as will be discussed in Chapter 8, where we propose to include vertical variations of the specific heat. The basic model used in this project is the "Unified Model" from the United Kingdom Meteorological Office (version 4.5.1), which is used mainly for Earth climate research and for weather forecasting.

The main challenge in my DPhil project is to simulate the atmospheric super-rotation for slowly rotating "worlds" such as Venus and Titan, and have a better understanding of the phenomenon, as said above. The circulation of these atmospheres have been studied by several models, Chapter 3, but is still not fully understood.

The super-rotation for the upper atmosphere for both Titan and Venus, amongst several hypothesis, is expected to follow the GRW theory where the super-rotation is caused by a net upward transport of angular momentum by Hadley-like circulation, with large scale barotropic eddies being the main transporter of momentum towards the equator (Gierasch (1975) and Rossow and Williams (1979)).

Recent work in Oxford has resulted in the development of a simplified general circulation model (SGCM) of the Venus atmosphere, which is already capable of quantitatively

reproducing some aspects of its meteorology (Lee, 2006). We now plan to develop a more complete GCM for the atmosphere of Venus. Amongst some modifications proposed in the project for the Oxford Venus GCM, we are implementing a new radiative scheme based in Net-Exchange rates matrix for the IR and table values for short-waves (see Chapter 6). The validation of the results will be done with observational data from Venus Express for Venus, and also from other results from successful GCMs. This Full GCM will allow a more careful study of the role of the clouds in the circulation of Venus atmosphere and its distribution.

The Simplified General Circulation Models (SGCMs) do not try to use fully Physics-base representations of all physical process. However, they are very useful tools in comparative studies of the different atmospheric circulations, since it is easier to adapt the model to different conditions and where the aim is more concerned with the dynamic features of the atmosphere. Adapting the well established Venus SGCM from Lee et al. (2007) for Titan's conditions, enables us to do comparative simulations and explore possible roles for waves and seasons in simplified forms. This will improve our tools to understand the atmospheric's circulation, and phenomena such as the super-rotation.

1.3 Report Summary

In the next Chapter, I will give an overview of the general characteristics for Venus and Titan namely the bulk and orbital parameters, surface, atmospheric composition and clouds, thermal structure and energy balance, and especially atmospheric dynamics.

Chapter 3 describes the state of the art regarding general circulation models for Venus and Titan.

On Chapter 4 the previous model developed for Venus is presented and on Chapter 5 new diagnostics are computed to study mixing barriers and the importance of eddy momentum fluxes in the upper atmosphere on this model.

Chapter 6 outlines the new radiative scheme which is being implemented in the Venus GCM and shows some diagnostics with that new parameterisation.

Chapter 7 presents the new Oxford Titan GCM, which has similar structure to the previous Venus GCM developed in Oxford in 2006. It shows some results from its early spin-up phase.

A general conclusion of my first year and a brief summary about my future work are presented in Chapter 8.

CHAPTER 2

General Characteristics of Venus and Titan

Contents

2.1 Venus

Venus is the second closest planet to the Sun, has no moons, and it is the most Earth-like astronomical object in our solar system (see Table 2.1). Despite this similarity, Earth and Venus have very distinct characteristics. To explain this, if we assume that at their formation the composition was the same, they must have had a different evolution. The physical mechanism by which Venus evolved still remains poorly understood.

Galileo Galilei observed Venus for the first time using a telescope in 1609, and later on, in 1631, Johannes Kepler mapped its orbit around the sun and observed the first transit of Venus. These were early discoveries about the planet that hid its rotation velocity in the dense layers of its atmosphere for more than 200 years. The first attempts to calculate the rotation velocity were made by Jean-Dominique Cassini between 1666 and 1667 and suggested a period of less than one Earth day from the observations of bright areas in the Venus atmosphere. Several scientists tried in the 18th and 19th century to obtain an accurate result for the Venus rotation period, but these measurements had difficulties such as: finding points of reference in the planet and short period of time to observe Venus from the telescopes. All the results obtained a rotation for Venus around 24h, but the observations from 1877 to 1878 by Giovanni Virginio Schiaparelli did not show any signal

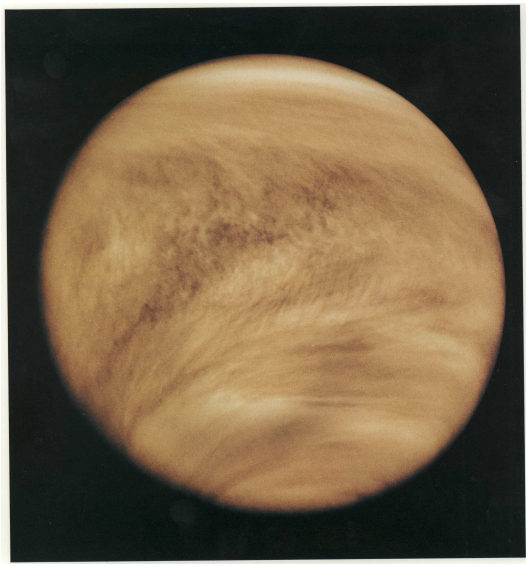

Figure 2.1: Ultraviolet image of Venus' clouds obtained by the Pioneer Venus Orbiter (Feb. 26, 1979).

of variation related with rotation. Based on its results Giovanni suggested that the rotation was synchronised with the movement around the sun, 224.7 days. This idea was against the value of a period of rotation of 24h shared by several scientist of his time. The true value was only found in the 20th century, using radar measurements which allows the radiation to penetrate in the thick atmosphere and have more accurate results for the rotation of the planet. The observations in 1962 by the Jet Propulsion Laboratory (NASA, EUA) obtained surprisingly a rotation in the inverse direction and very slow, with a period of 240.0 days (Goldstein (1964) and Carpenter (1964)). Combining the period of rotation with the orbital period of 224.7 days, one get a Solar day on Venus of 116 days, with the Sun rising in the west and setting in the east.

Understanding the origin of the mysterious retrograde rotation, opposite to most of the other bodies in the Solar System, has been a challenging problem. In Correia and Laskar (2001), it is explained that the actual state of the retrograde rotation of Venus is not from primordial origin (in the formation planet/solar system), but from the post-formation dynamical evolution. The inclination of the rotation axis of the interior planets is a degree of freedom with irregular movement due to the coupling of rotation itself, with perturbations due to the movement of other bodies in the solar system.

The slow retrograde rotation coupled with an orbit of eccentricity almost zero and a low spin axis inclination leads to a very weak seasonal variation on Venus.

Despite being called Earth's "sister planet", because of the similar size, gravity, and bulk composition, Venus has the most massive atmosphere of the terrestrial planets, covered by an opaque layer of highly reflective clouds preventing its surface from being seen from space in visible wavelengths. The main gas of its atmosphere is CO_2. In the Earth this gas can be efficiently removed from the atmosphere dissolving into oceans, but in Venus it is the major cause for the high temperature in the atmosphere and surface. CO_2 as a

"greenhouse" gas and being the main component of the atmosphere (Venus contains a total of about 92 bars of CO_2), raises the surface temperature to about 750 K, three times higher than if this effect did not exist in Venus. The clouds mainly composed by droplets of sulphuric acid have a total mass relatively small but enough to contribute to the planet's visible appearance (see Figure 2.1), atmospheric thermal structure and energy balance.

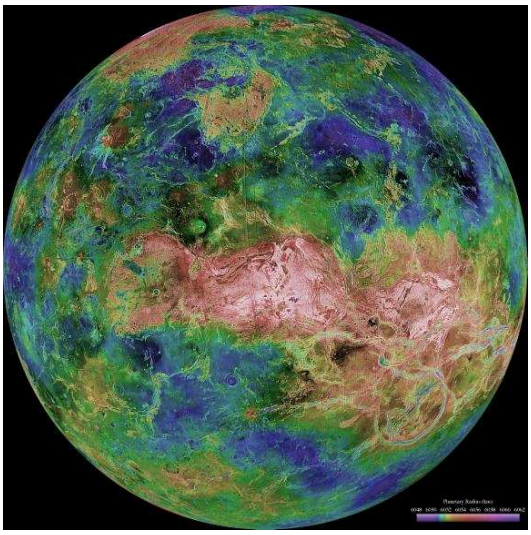

Figure 2.2: Radar map of the surface of Venus measured by Magellan probe (1990's). The red colour represents the highest levels and blue the depressions. The north pole is at the center of the image.

2.1.1 Surface

The first estimate of the temperature on the Venus's surface was in the 1950's, with the possibility to measure the intensity of the microwave radiation coming from the planet using radio telescopes. The value obtained was around 673 K, and it was confirm by the probe Mariner 2, that showed the surface as the source of this radiation. Later, the Venera landers measured a temperature of roughly 730 K, showing a sterile, mainly basaltic, surface like a scorched desert dominated by a rock-strewn landscape. Some questions related to the composition, the transformations that the rocks suffer in the surface and the process of erosion still remain unanswered.

The satellite Magellan mapped the planet's surface from orbit and showed that the planet Venus is 70% covered by smoothly (rolling) plains, 20% of low lands and the last 10% highland regions, see Figure 2.2. Apparently the movement of tectonic plates seems to not exist, and the cause of the formation of highlands, which appear as massive local mountains, is suggested to be caused by a deep process within the crust, like a vigorous convection in a large "hot spot" in that zone. Much of Venus's surface appears to have been shaped by volcanic activity. This "renews" the surface, making it look relatively young. The several hundred craters in the surface are uniformly distributed and in a well-preserved condition (an indication for the resurfacing phenomenon). The size of the craters is related with the filtering of the huge atmosphere that covers the planet, which does not allow the formation of small meteoric craters.

	Venus	Titan	Earth
Mean Radius (km)	6051.8	2575.0	6371.0
Surface gravity (equator ms^{-2})	8.87	1.35	9.78
Bond Albedo	0.75	0.2	0.306
Solar Irradiance (Ws^{-2})	2623.9	14.90	1367.6
Black-body temperature (K)	231.7	84.5	254.3
Sidereal orbit period (days)	224.701	(15.95)	365.256
Tropical orbit period (days)	224.695	(15.95)	365.242
Orbit inclination (deg)	3.39	27 (relative to Saturn)	0.0
Orbit eccentricity	0.0067	0.029	0.0167
Sidereal rotation period (hrs)	(-)5832.5	382.68	23.9345
(Solar) Length of day (hrs)	2802.0	383.68	24.0
Solar day / Sidereal day	0.480411	(1.000)	1.000274
Obliquity of orbit (deg)	177.36		23.45
Surface Pressure (atm)	92	1.5	1
Mean molecular weight (g/mole)	43.45	28	28.97
Gas constant (J/K/kg)	188	290	287
Specific heat (J/K/kg)	850.1	1005	1005
κ=R/C_p	0.222	0.277	0.286
Atmospheric composition	0.95 CO_2	0.9-0.97 N_2	0.78 N_2
	0.035 N_2		0.201 O_2
Global Super-rotation	10	6-10	0.015
Local super-rotation (maximum)	60		3-8
Sidereal day (Earth days)	243	1.025	1
Solar Days (Earth days)	116.95	1.027	1.000274
Surface Temperature (approx K)	730	94	285

Table 2.1: Table from Lee (2006) with the bulk, orbital and atmospheric parameters for Venus (Williams, 2003), Earth (Williams, 2003) and Titan (Coustenis and Taylor (1999) and Allison and Travis (1985)).

Total mass of atmosphere	4.8×10^{20}kg
Mean molecular weight	43.45 g/mol
Scale height	15.9km
Atmospheric composition (near surface, by volume)	
Major	Carbon dioxide (CO_2) 96.5%
	Nitrogen (N_2) 3.5%
Minor (ppm)	Sulphur dioxide (SO_2) 150
	Argon (Ar) 70
	Water (H_2O) 20
	Carbon monoxide (CO) 17
	Helium (He) 12
	Neon (Ne) 7

Table 2.2: Venus atmospheric composition (Taylor, 2006)

2.1.2 Atmospheric Composition and Clouds

Venus has a dense atmosphere mainly composed of Carbon dioxide ($\sim$96.5%) and a small amount of nitrogen ($\sim$3.5%), Table 2.2. It is observed in the atmosphere that some times, the minor constituents like sulphur dioxide, carbon monoxide and water, exhibit local concentrations with temporal and spatial variations, which are linked with its atmospheric circulation and meteorology, and/or some occurrence in the surface like volcanism. The images in the UV (see Figure 2.1), show a dominant pattern in the atmosphere with the shape of the letter "Y" or the inverse "C", laid sideways. This feature is related with some unknown UV absorbent substances that are redistributed spatially by the dynamics on the atmosphere.

The main cloud deck is composed mostly by sulphur dioxide and sulphuric acid droplets and it extends from about 45 to 65 km above the surface, with haze layers above and below. At the UV, visible and most of the infrared wavelength range, the clouds are very thick, hiding completely the surface of the planet. The clouds have particles of three different modes whose proportions are different in the different layers, with sizes ranging from less than 1 to over 30 μm in diameter. The smaller particles, 'mode 1' droplets, extend throughout the top of the clouds and their composition is still unknown. The droplets of the 'mode 2' are mainly H_2SO_4 and H_2O, and the 'mode 3' are probably composed by "bigger droplets" of H_2SO_4 and are located at lower and mid cloud layers.

The clouds have a very high optical depth and a high single scattering albedo in some of the most significant spectral intervals, but they are not completely opaque to all wavelengths: some visible and near-IR spectral windows can be observed.

From the near-IR mapping spectrometer (see Figure 2.3), it is possible to observe variability on the horizontal and vertical structure of the clouds, which is a consequence of the dynamical transport and the production and destruction of particles in the clouds.

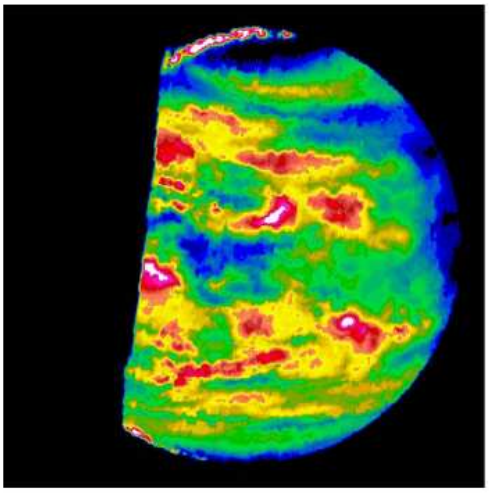

Figure 2.3: This false colour image is from the night side of Venus in the near-infrared 'window' at 2.3 μm, and was obtained by the NIMS aboard the Galileo spacecraft during its flyby in February 1990 (Carlson et al., 1991). The variations (more than one order of magnitude) in brightness show the change in thickness of the clouds from white and red (thin cloud regions) to black and blue (thick clouds).

2.1.3 Thermal Structure and Energy Balance

In the case of planets without an internal source of energy, the Sun is the main source of energy. If Venus was an airless planet with an albedo of 0.76 and having the same distance from the sun, the expected value for the surface temperature would be around 230K, which is very different from the value observed. One possible cause for the discrepancy in the values is related with the composition of the massive atmosphere in Venus that creates a significant greenhouse effect. This feature is responsible for the high temperatures at the surface. The lower atmosphere (troposphere), due to the large opacity of the overlying layers, does not radiate enough energy at long thermal wavelength to space. It re-emits part of the energy received back to the surface, raising its expected temperature (to around 730K).

The atmosphere of Venus is more efficient transporting heat from the equator to the poles than the planet Earth. This feature has influence in the gradient of the net thermal emission that is stronger in Venus (see Figure 2.4) due to the high thermal capacity and to the more "organised" atmosphere in a less turbulent regime.

The clouds have a very important role in the thermal structure of the atmosphere since it absorbs and reflects the major part of the solar flux radiation and contributes as well for the "greenhouse" effect. Due to the highly reflective properties of the clouds, the planet receives less total solar energy than the Earth.

Computing the height and the density from the accelerometer measurements of the Pioneer Venus entry probe,the values of different temperature profiles for different locations were retrieved from the hydrostatic equation complemented with the equation of state. In

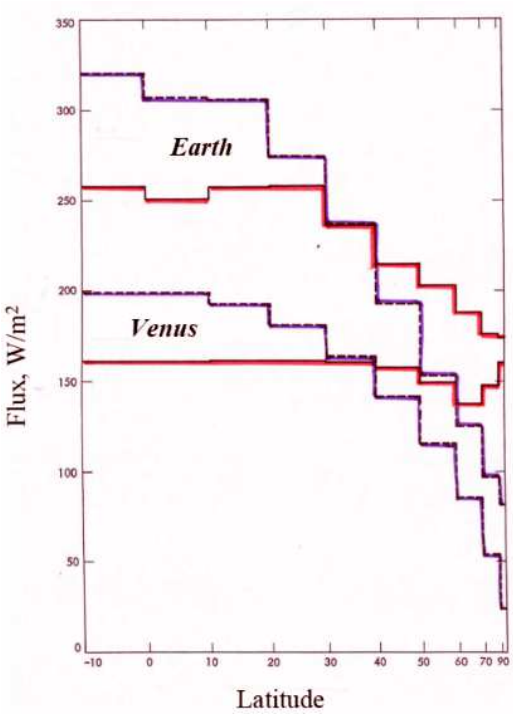

Figure 2.4: The purple lines represent reflected solar flux and the red lines the thermal flux in Earth and Venus. Image from Crisp (2007).

Figure 2.5, four vertical profiles of temperature are shown (Seiff et al., 1980), plus one that was used in the thermal forcing of the Oxford Venus GCM (Lee, 2006). The radiative time scales which are needed as well in the parameterisation can be calculated using radiative models (Pollack and Young, 1975). However, the values used in the GCM are less than the values obtained for almost every altitude. This difference is mainly related to computation cost and an advection mechanism that was neglected in the radiative calculations in Pollack and Young (1975).

2.1.4 Atmospheric Dynamics

The circulation of the atmosphere in Venus (see Figure 2.6) is governed by two regimes for different structures in the atmosphere: the retrograde zonal super-rotation in the troposphere and mesosphere (Gierasch et al., 1997), and the solar-antisolar circulation across the terminator in the thermosphere (Bougher et al., 1997). Several observations done by descent probes, Vega balloons or using cloud tracking in the UV, showed that in the troposphere (0 to around 70km), the winds reach a maximum of 100ms^{-1} at the cloud tops and decreasing to roughly zero at the surface (Figure 2.7). In average, the main cloud deck rotates around the planet in a period of 4-5 days, being around 50-60 times faster than the rotation of the slowly solid body, maximum of 2ms^{-1} at the equator relative to the background stars.

The dynamics of the atmosphere in Venus is driven by a differential insulation in lat-

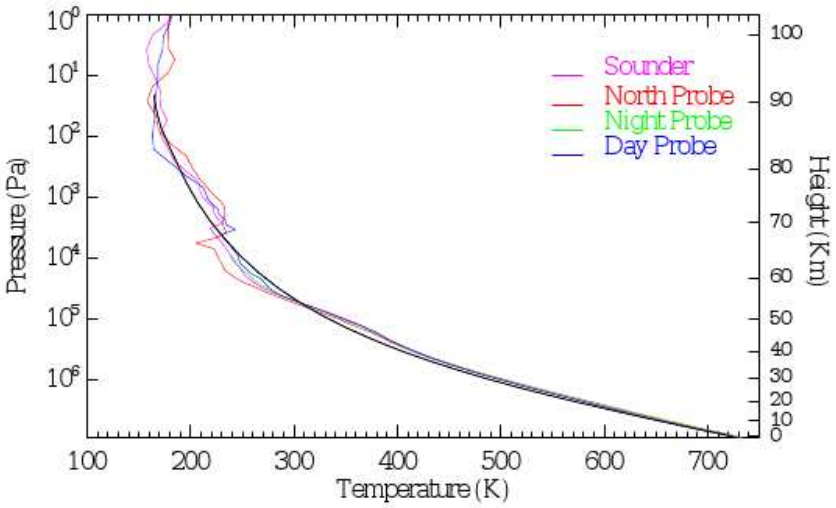

Figure 2.5: The black line is the temperature profile used in the thermal forcing of the Venus GCM (Lee et al., 2007). The figure was obtained from Lee (2006) which used the data from Pioneer Venus descent probe (Seiff et al., 1980). The night probe measured the temperatures up to 65 km only. The four probes obtained the data from different latitudes and local times: Sounder - 4.4° N, 7:38 am; Day - 32.1° S, 6:46 am; Night - 28.7° S, 0:07 am; North - 59.3° N, 3:35 am.

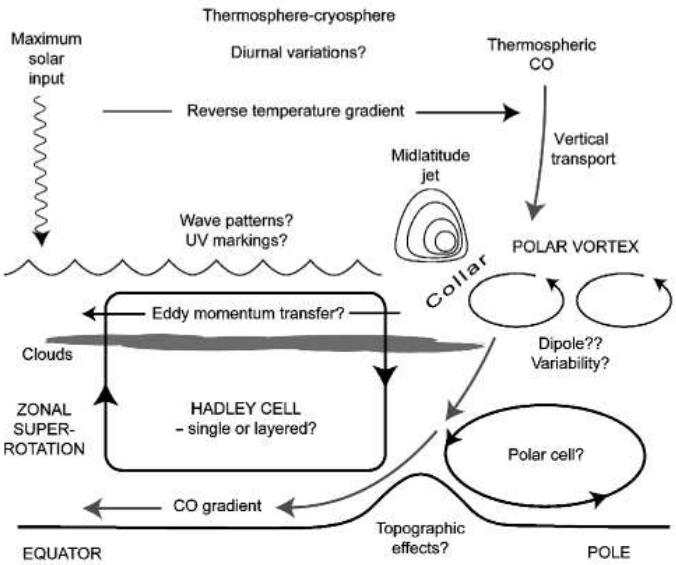

Figure 2.6: The figure summarises schematically the main features of the atmospheric circulation on Venus and some questions that remain poorly understood (Taylor, 2006).

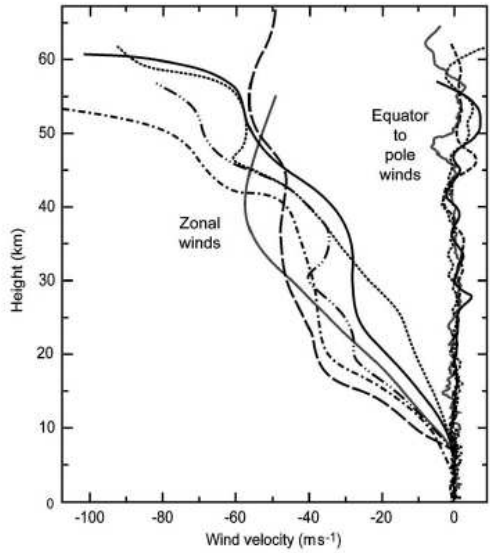

Figure 2.7: Venus wind profiles (Height-Wind velocity) from the Pioneer Probes (Taylor, 2006).

itude, and the presence of middle or high latitude super-rotation is well explained as a consequence of poleward angular momentum transport by a thermally direct Hadley circulation. More difficult to explain, is the presence of the observed equatorial super-rotation in its atmosphere. Such a phenomenon requires the presence of nonaxisymmetric eddy motions, because the flow in this zone rotates with much higher angular velocity than the one driven by a differential insulation planetary rotation under just the existence of axisymmetric circulation, unless super-rotation was its initial condition. There are several mechanisms that can explain the formation of such eddies: barotropic instability of a high-latitude jet produced by the Hadley cell (Gierasch (1975) and Rossow and Williams (1979)); transient or topographically forced planetary or small-scale gravity waves (Leovy, 1973); Solar semidiurnal thermal tide (Fels and Lindzen, 1974); and external torques (Gold and Soter, 1971).

The observations in the IR made by Venus Express showed a bright south pole surrounded by a cold "collar" (Piccioni et al., 2007), that is very similar to what was observed in previous missions to the north pole (Taylor et al., 1979) (see Figure 2.8). These huge cyclonic structures change their central morphology continually, showing a single, double or tri-pole structure that rotates around the pole. Analysing in altitude, there are two phases that characterise the polar vortex: at about 50 km, a cold "collar" circulating around a higher temperature polar cap, and at about 90 km, the warm pole, where the temperature of the pole is higher than the equatorial one.

The nature and mechanisms of the polar temperature structures and the polar vortices are still not clear. It has been proposed that the polar temperature structures are a result of the compressional adiabatic warming from the descending branch of the meridional cell circulation, coupled with variations in the solar heating, due to variations in the haze

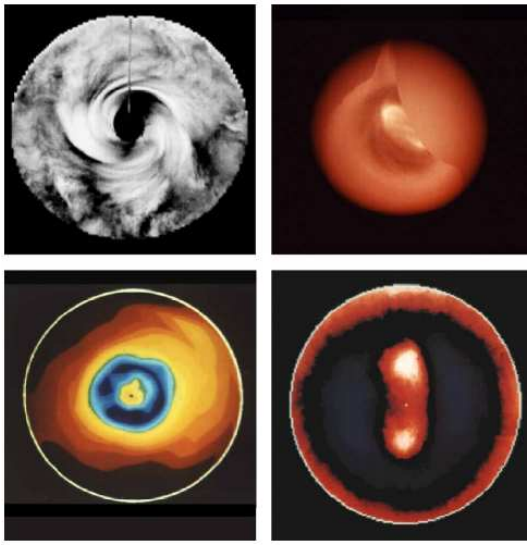

Figure 2.8: The figure shows four images of the North polar vortex (Taylor, 2006). The one in the top left, is a UV image from Marine 10, the bottom left one was taken at 11.5 μm with Pioneer Venus and shows the cold "collar" (Taylor et al., 1980). The top right image is averaged over 72 days, and shows the dipole structure surrounded by a cold "collar". The last image is about the collar-dipole structure again, which remains poorly understood.

densities at 80 km. The dynamics of the polar vortices in Venus seems to be related to the possibility of barotropic instabilities in the polar flow (Limaye et al., 2009).

The global waves activity in Venus' atmosphere is likely to play an important role in the transport of momentum and energy in the atmosphere. The planetary-scale cloud patterns observed in the UV measurements, with a shape of a large horizontal "Y", can be explained by the presence of atmospheric waves travelling slowly with respect to the cloud-top winds. The combination of mid latitude waves travelling somewhat slower than the winds, interfering with slightly faster equatorial waves coupled with some non-linear effects can explain the pattern observed. The real nature of the waves in the atmosphere of Venus is difficult to explain due to the lack of observational data. del Genio and Rossow (1990) studied the images from UV to study the characteristics of the waves in the atmosphere of Venus, and correlated the contrasts of an unknown absorber ("Y" and reversed "C" shape), the winds and the temperature fields. The waves observed at 65-70 km of altitude were of two types: equatorially trapped waves moving in the same direction as the wind but faster, extending from its equator to roughly 20° latitude and with a period of 4 days, identified as a Kelvin wave; mid-latitude waves moving in the same direction of the winds but slower, with two different periods of 4 and 5.2 days, which were intrepreted as Mixed-Rossby-Gravity waves (del Genio and Rossow, 1990).

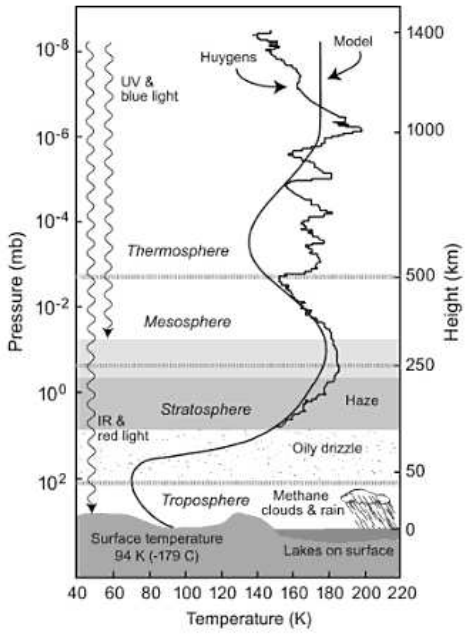

Figure 2.9: The figure shows schematically some features of Titan's atmosphere such as the temperature, clouds, hazes, precipitation, surface, and radiation fluxes. This figure is taken from Coustenis and Taylor (1999). The smooth temperature profile curve is from a theoretical model done before the Cassini mission (Yelle et al., 1997), and the Huygens temperature profile is from Fulchignoni et al. (2005).

2.2 Titan

In 1655 the Dutch astronomer Christian Huygens discovered the first known moon of Saturn, Titan (see Table 2.1). Titan is the largest moon of Saturn, and the only moon in the Solar System to have a thick atmosphere, which caused an overestimation in measuring its dimensions before the arrival of Voyager 1 in 1980. It is a cold world (surface temperature is around 94 K) covered by an atmosphere mainly composed by nitrogen, like the Earth, but having methane as other of the main constituents, Figure 2.9.

As the Earth's moon, Titan is tidally locked in synchronous rotation with a planet, orbiting once every 15.94 days in a positive direction at a distance of about 1.2 million kilometres. A small satellite called Hyperion, is locked in a 3:4 resonance with Titan, which could have been captured by the moon from a possible chaotic trajectory.

The moon has an equatorial radius of 2575km, which makes Titan the second largest in our solar system (Jupiter's moon Ganymede is 112km larger). The value of the mean density is around 1.88 g/cm^3 suggesting that the composition of Titan is half water and half rocky material compressed due to gravitation.

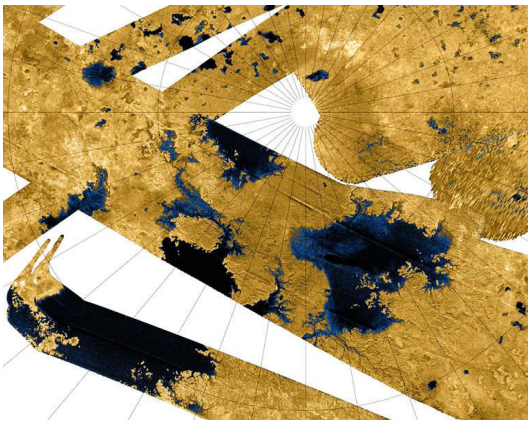

Figure 2.10: This figure shows a Cassini false-color mosaic with all synthetic-aperture radar images to date of Titan's north polar region. The regions with the colours in blue and black are related with liquids (hydrocarbon lakes).
Copyright NASA/JPL/USGS

2.2.1 Surface

The satellite Cassini, which was prepared to float in hydro-carbonates like methane and ethane because it was thought that the surface was almost completely or fully covered by an ocean. After its launch other reality started to become more plausible, with a surface with little or no liquid. Later, after the arrival of Cassini and the landing of Huygens, it was discovered that the surface of Titan was in an intermediate state due to the observation of geological structures related with the presence of liquids, like rivers and lakes of methane and ethane (Stofan et al., 2007) (see Figure 2.10). The confirmation arrived on June 2008 with the data from Cassini's Visible and IR Mapping Spectrometer (VIMS) about a liquid in a Lake Ontario in Titan's southern hemisphere (Brown et al., 2008).

The surface of Titan is relatively smooth, the observations obtain roughly height variations of the order of 150 m and the mountains have less than 2 km. The small number of craters suggests a relatively young surface influenced by geological processes like: erosion by winds, slushy volcanoes, as well as hydrocarbon rain and soot, depositing possibly new material on the surface. Other feature of the moon that certainly is reducing the number of craters is its massive atmosphere, that acts as a shield. It was estimated that the number of craters is reduced by a factor of two due to atmospheric shielding (Ivanov et al., 1997).

There is some evidences of volcanic activity (cryovolcanism) in Titan. The cryovolcanism, which is suspected to exist in Titan and highly possible to exist in many other frozen bodies in the solar system, consists in a volcanic process involving icy fluids (water in Titan's case), or cryolavas that is water or water-ammonia, which behave similarly to basaltic lavas on Earth. This phenomenon, that can be a source of methane in the atmosphere, needs heat to activate. There are some suggestions for the origin of the heat source, for example, the decay of radioactive elements within the mantle.

Constituent	Mole Fraction
Major	
Molecular nitrogen, N_2	0.98–0.82
Methane, CH_4	2×10^{-2} (at 100 mb)
	$(8\pm3)\times10^{-2}$(at 3700 km)
Minor	
Argon, AR^{36}	$<6\times10^{-2}$ (at 3900km)
Hydrogen (molecular), H_2	$(2\pm1)\times10^{-3}$
Hydrogen (atomic),HI	$<10\%$ (at 3900 km)
Neon, NeI	$<1\times10^{-2}$
Ethane, C_2H_6	2×10^{-5}
Carbon monoxide, CO	6×10^{-5}

Table 2.3: Atmospheric Composition of Titan (Atreya (1986), Broadfoot et al. (1981), Hanel et al. (1981), Samuelson et al. (1981), Smith et al. (1982), Strobel and Shemansky (1982), Lindal et al. (1983) and Lutz et al. (1983)).

2.2.2 Atmospheric Composition and Clouds

The atmosphere of Titan is mainly composed by nitrogen, N_2 (see Table 2.3), more than 90%. Cassini/Huygens missions, detected and measured the major constituents, improving the results of the last missions. It was confirmed the methane as the second most abundant, with a mole fraction of 1.41×10^{-2} in the stratosphere, increasing until about 8 km, 4.9×10^{-2}. This large value is probably related with condensation of the methane at those altitudes.

These two major components of the atmosphere (nitrogen and methane), are both photo-dissociated by different sources: galactic cosmic rays, solar ultraviolet radiation and energetic particles from Saturn's magnetosphere. This mechanism is responsible for the complex organic photochemistry which produces the haze.

Cassini and Voyager missions determined that the molecular hydrogen (the third most abundant) is within a range of 0.1-0.2%, where in the presence of aerosols and atomic hydrogen more H_2 is created. Other significant constituent of its atmosphere is the only noble gas detected until now, Argon, which was found in small amounts in two types: primordial ^{36}Ar (mass fraction of 2.8×10^{-7}) or its radio isotope ^{40}Ar (4.32×10^{-5}).

In December 2001, observations from a ground based telescope at the summit of Hawaii's Mauna Kea, detected directly for the first time methane clouds in Titan (Brown et al., 2002). The images obtained showed bright clouds near Titan's south pole, constantly changing its intensity, demonstrating the existence of condensation and localized moist convection in Titan's atmosphere. Later in 2006, Cassini observed large clouds at an altitude of 40 km over the north pole. The clouds detected were composed of methane, ethane an other organic compounds.

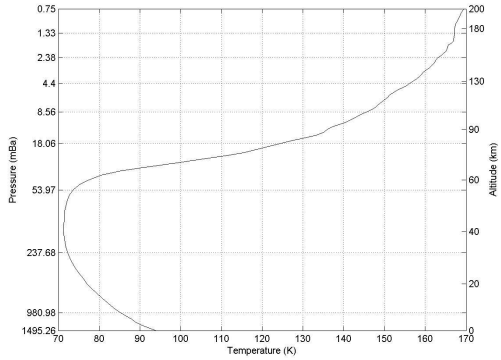

Figure 2.11: Reference temperature profile used in the thermal forcing for Titan GCM derived from observational data (Lindal et al., 1983).

2.2.3 Thermal Structure and Energy Balance

The cold moon of Saturn, Titan, absorbs the major part, $\sim$60%, of the incident solar energy before it arrives at the surface, and $\sim$30% is reflected back to space. The high levels of Titan's atmosphere absorb mainly the shorter wavelengths by processes such as ionisation and dissociation of atmospheric gases. The longer wavelengths, coming from the sun or re-emitted by the surface and the atmosphere as well, are absorbed by the minor constituents like methane, which has an important IR spectrum due to the internal charge distribution that forms a net dipole moment. This last phenomenon makes the atmosphere very opaque to the IR radiation. Other contribution to the opacity at long-wavelengths is the collision between molecules of N_2, which is the main gas in the atmosphere, which produces temporary dipole moments (collision-induced).

Assuming that Titan is in radiative equilibrium, it is possible to do a simple calculation for the temperature of the surface. Using the Stefan-Boltzmann law and the 228 megawatts that falls on Titan from the Sun, minus the amount reflected ($\sim$30%) and using an approximate correction for the extra amount received from near surface atmosphere which absorbs IR, is possible to obtain a temperature of 94.4 K. The value from this simple approximation is close to the one obtained by the Huygens probe.

The Figure 2.11 shows a vertical temperature profile, which is the one used for the vertical temperature reference in the parameterisation of the thermal forcing used later in the Titan SGCM (see Chapter 7). The figure indicates some properties of the different atmosphere's structure up to the stratosphere.

In Flasar et al. (1981), it is suggested from infrared measurements of the spatial distribution of temperature that there is no relevant latitudinal or diurnal variations of the temperature for any altitude of the lower atmosphere, which is reinforced by the large values of radiative constant times calculated for Titan's atmosphere. In the upper stratosphere, the meridional contrasts are approximately 20 K where the radiative time constant is shorter.

Property	value
Surface	
Pressure	1496±20 mba
Temperature	94±0.7 K
Effective temperature	86 K
Measured lapse rate	
0–3.5 km	1.38±0.1 K km^{-1}
3.5 km	0.9±0.1 K
42 km	0
Troposphere	
Height	42 km
Pressure	127 mba
Temperature	71.4±0.5 K
Stratosphere	
Height	200 km
Pressure	0.70 mba
Temperature	170±15

Table 2.4: Table from Atreya (1986). The data are from Lindal et al. (1983).

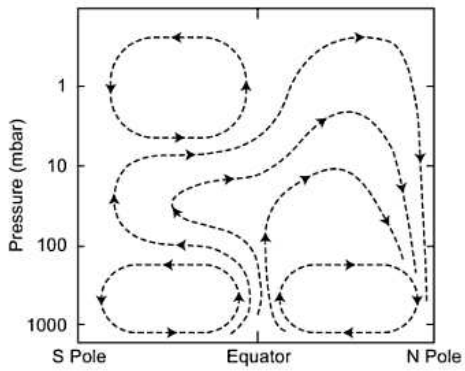

Figure 2.12: A suggested scheme for Titan's general circulation for northern spring (the general picture is largely dependent of the season) which was proposed by Flasar et al. (1981).

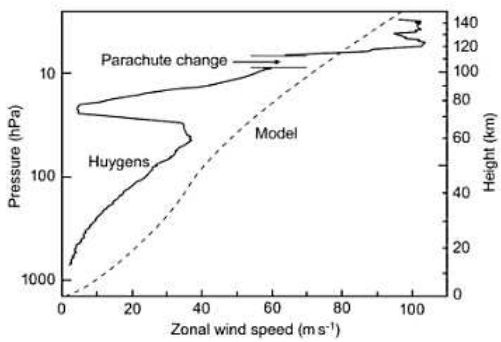

Figure 2.13: Zonal wind profile obtained by Huygens probe (Bird et al., 2005). The smooth curve was obtained using a zonal wind model by Flasar et al. (1997).

2.2.4 Atmospheric Dynamics

The nature of Titan's general circulation is still poorly known, there are few data available in comparison with the other terrestrial planets of our solar system. The study of other atmospheres has helped to understand the dynamics of Titan's atmosphere, applying the Universal laws of atmospheric physics and fluid dynamics (see Figure 2.12).

Titan rotates slowly in a positive direction, and its atmospheric zonal winds have been suggested by the haze's rapid zonal motion, to be cyclostrophic in the same direction of the planet's rotation, which is similar to Venus. Assuming this balance, it is easy to retrieve the zonal wind from temperature fields. From Cassini data of 2004, it was possible to measure the weakest values for the winds at high southern latitudes, which increased toward the north. The maximum value obtained was 160 ms^{-1} at 20-40°N. From Huygens probe which entered at 10°, it was possible to measure accurately, the vertical profile of the zonal winds, which showed values smaller than the values obtained by numerical models and an interesting feature as a valley between the 60 and 100 km (see Figure 2.13).

It is possible to verify from Figure 2.13, that for some areas of the atmosphere, we observe zonal velocities that are a clear feature of super-rotation of the atmosphere comparing with solid body rotation rate of 16 days, which seems to be very similar to Venus' case - a slowly rotating body with an atmosphere in rapid rotation. One possible explanation for this super-rotation is from the Gierasch-Rossow mechanism (there are several mechanisms listed in the Venus dynamics atmosphere section). This mechanism suggests that a barotropically unstable high latitude jet is produced by the upward and poleward angular momentum transports by the mean meridional circulation (Large Hadley Cell), which with equatoward eddy momentum flux maintains the equatorial zonal wind.

The inclination of the rotation axis angle with the ecliptic plane (roughly 27°) is responsible for a strong seasonal variation that possibly affects largely the form of the Hadley cell, as was obtained in a numerical study by Hourdin et al. (1995). During most part of the year in Titan the Hadley cell extends from pole-to-pole, where the symmetric two-cell configuration seems to appear in a limited transition period in the equinoxes.

In the troposphere, the geostrophic balance is a better approximation than the cyclostrophic, due to the weaker velocity winds. As a result of the geostrophic balance and the pole-to-pole Hadley cell, the zonal winds change their direction depending on the season and in each hemisphere.

The wave activity in the atmosphere is thought to be important to maintain the super-rotation atmosphere. Despite of few direct evidence of wave activity, Rossby waves are expected to be present in the atmosphere, the ones related with the "Y" shape observed by UV measurements in Venus. Due to the type of atmospheric circulation, the barotropic waves are expected to exist and to transport momentum from high to low latitudes.

The proximity and the eccentric orbit of Titan around Saturn, cause the non-axisymmetric gravitational tides. This phenomenon causes a periodic (16 days) atmospheric pressure perturbation in the atmosphere, and has a relevant effect in the lower atmosphere where it introduces a maximum amplitude perturbation of the order of one tenth in temperature and unity in the winds (Tokano and Neubauer, 2002).

CHAPTER 3

General Circulation Models for Venus and Titan

Contents

3.1 Venus

3.1.1 Venus GCMs

General Circulation Models (GCM) applied to the planet Venus have become important tools for understanding its atmospheric dynamics, and are being developed now by several groups across the world. These numerical simulations study the dynamics, by integrating numerically the equations of hydrodynamics on the sphere, using thermodynamics for various energy sources.

The improvement of the dynamical core of the GCM and the improvement in computer technology brought advances and better results for these computationally expensive models. The adaptation made in these models for the Venus' atmosphere presents some technical difficulties regarding accuracy and computation time, mainly associated with the radiative scheme within the massive atmosphere. Venus GCMs have been developed since more than three decades ago. They have typically used simple physical parameterisations or restrictions to less than three dimensions due to the difficulties highlighted above, but their success has been gradually increasing over the years. As part of this evolution, we find works such as those of Kalnay de Rivas (1975), based on a simple quasi-three-dimensional spectral model and which produced a weak super-rotation, with a maximum westward wind speed of 20 m s^{-2}, which was pointed out later by Mayr and Harris (1983) as having an inappropriate parameterisation of the thermal conductivity.

3.1.2 Recent Venus GCMs

Nowadays, the formulation of numerical circulation models is being developed at several institutions around the world, including: France (Lebonnois et al., 2009), USA (Hollingsworth et al. (2007), Parish et al. (2008)), Japan (Ikeda et al., 2007) and UK (Lee et al., 2007).

The Oxford model is among the leading "Simplified GCMs" - i.e. models which do not try to use fully Physics-base representations of all physical process, but include simplified representations of heating, cooling and friction processes (Lee et al., 2007). This has led to some success in producing plausibly realistic Venus-like global circulations, with a significant super-rotation (within a factor of 2).

To date, the French (LMD, Paris, France) GCM, Lebonnois et al. (2009) and the Japanese (CCSR/NIES/FRCGC) GCM, Ikeda et al. (2007), are the only two that attempt to include a full radiative transfer model that computes temperature structure self-consistently. This is particularly challenging because of the extreme opacity of the atmosphere in the IR. The method used in the LMD group is based on the parameterisation developed by Eymet et al. (2009), that uses a Net Exchange Rates formulation. The CCSR model uses a two-stream radiative scheme (Nakajima et al., 2000).

These two models are the most recent successful models, and seem capable of showing a super-rotation above the clouds, similar to observations. Below the clouds, the results are not so promising since the observed variation with height of the super-rotation is not obtained, starting from a initial condition of a rest atmosphere. In the chapter regarding the radiative scheme (similar parameterisation to the one used in the GCM of the LMD group), it is possible to observe in the results that the mid atmosphere is heating from the hot lower atmosphere, which creates a zone of convection. The cooling to space appears to be stronger at the upper atmosphere inducing thermal instabilities. There are several points to be investigated in these models, as for example the role of the thermal tides which seem to be important to maintain a strong equatorial super-rotation in the LMD GCM, supporting the Gierasch mechanism (Lebonnois et al., 2008), the influence of variations of the specific heat with temperature, the role of the topography and the potential role of sub-grid scale gravity waves.

3.2 Titan

3.2.1 Titan GCMs

The atmosphere of Titan has been investigated with general circulation models. Amongst the existent models, the ones at which I will give more emphasis are Hourdin et al. (1995) and del Genio et al. (1993). The adaptation of terrestrial GCMs to other Earth-like atmospheres has had some success like in the case of Mars, Venus and Titan.

In the del Genio et al. (1993), they used a simplified Earth model with Titan's rotation rate, which produced strong winds in the same direction of the solid's rotation at the equator. The mechanism to produce the super-rotation in the atmosphere was suggested to follow the Gierasch mechanism (Gierasch, 1975), which is stronger in the presence of an optically thick cloud deck.

In Hourdin et al. (1995) the Gierasch mechanism is also suggested to be the responsible for producing the super-rotation which is produced spontaneously with prograde wind at the equator. The results showed little sensitivity in the troposphere and stratosphere due to the diurnal forcing, and the changes in the horizontal resolution are only relevant in the stratospheric super-rotation. The 3D model used was based on finite-difference representation, which computes the heating and cooling rates by a radiative scheme from McKay et al. (1989), and also includes a parameterisation for the vertical turbulent mixing of momentum and potential temperature.

There are more successful GCMs for Titan's atmosphere: the 2D (latitude-height) GCM from the LDM group, Rannou et al. (2005) that uses a parameterised up-gradient momentum transport; a 3D GCM from Tokano et al. (1999) which uses the radiative scheme from McKay et al. (1989) and includes also gravitational tide effects and an improved parameterisation regarding variations of the surface's temperature comparing with other models, but showing a weaker super-rotation in the stratosphere; more recently, the 3D GCM known as TitanWRF (Newman et al., 2008), includes a more recent version of the radiative scheme from McKay et al. (1989) and also diurnal and seasonal variations in solar forcing which is running efficiently on parallel machines.

CHAPTER 4

OPUS-V

Contents

The Venus SGCM used in this work was developed in Oxford (Lee, 2006), also known as OPUS-V (**O**xford **P**lanetary **U**nified **S**imulation model for **V**enus). This model was based in an advanced GCM for Earth (Cullen et al., 1992), and adapted for the study of the atmosphere of Venus (Lee et al., 2007).

4.1 The Model

The Venus GCM uses values of the physical and dynamical properties corresponding to Venus (Colin (1983) and Williams (2003)), and simplified parameterisation for radiative forcing and boundary layer dissipation. It is configured as an Arakawa B grid (Arakawa and Lamb, 1981), and adapted to use a 5x5 horizontal resolution covering the entire domain with 31 vertical levels, extended from the surface to an altitude of around 90 km, with a maximum of 3.5 km in the vertical grid spacing.

The radiation scheme used is not based in a radiative transfer model. Instead it used a linear thermal relaxation scheme towards a reference temperature which was obtained from Pioneer Venus probe data (Seiff et al., 1980), VIRA model, and a vertical contribution which reflects the peak in absorption of the solar insulation within the cloud deck. The interaction of the atmosphere with the surface was modelled by a boundary layer scheme with a linearised friction parameterisation. In the three upper layers, a sponge layer is included, with Rayleigh friction dumping horizontal winds to zero.

Using this simple GCM for Venus, it was possible to reproduce a super-rotating atmosphere without any non-physical forcing, diurnal or seasonal cycles. The result of the super-rotation is shown in the Figure 4.1a, where the horizontal equatoward transport of momentum at 40-80 km is responsible for maintaining the equatorial super-rotation.

The model reproduces equatorial Kelvin waves and Mixed-Rossby-Gravity (MRG) waves spontaneously, as shown in the Figure 4.2. Regarding the MGR waves, it was verified that they have an important influence in maintaining the equatorial super-rotation.

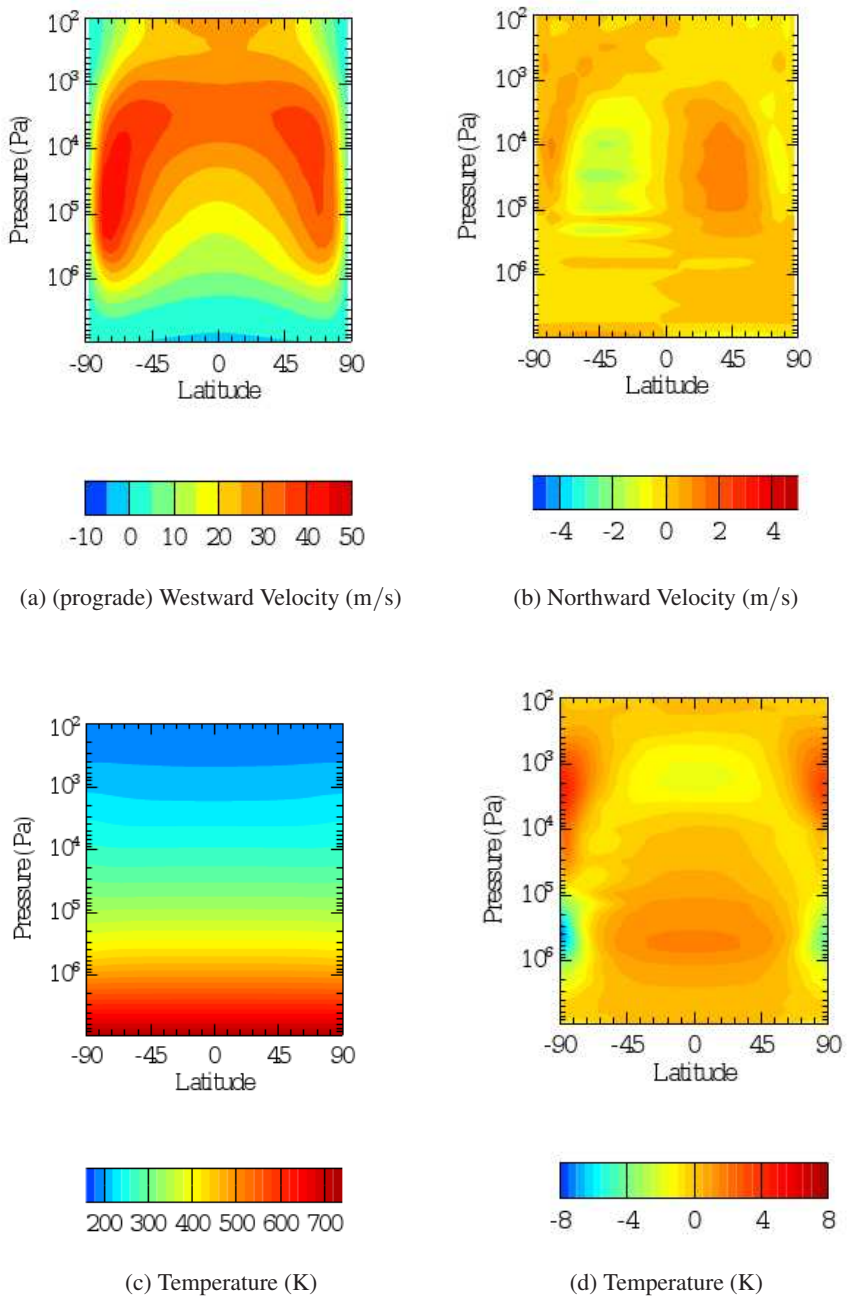

(a) (prograde) Westward Velocity (m/s)

(b) Northward Velocity (m/s)

(c) Temperature (K)

(d) Temperature (K)

Figure 4.1: Prognostic variable diagnostics after 500 days of zonal average from the Oxford Venus GCM, without the diurnal forcing and after 40000 Earth days of integration from a rest atmosphere (Lee, 2006). **(a)** Westward wind speed (m/s). **(b)** Northward wind speed (m/s). **(c)** Temperature(K). **(d)** Temperature after the latitude mean has been removed (K).

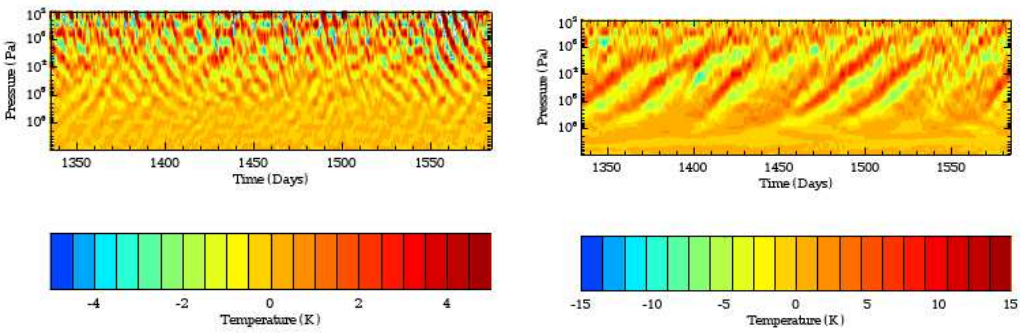

(a) Equatorial Kelvin waves

(b) Mixed-Rossby-Gravity waves

Figure 4.2: **(a)** Equatorial Kelvin waves with a period of 9.5±0.5 days and **(b)** Mixed-Rossby-Gravity waves with periods of 30±2 days are spontaneously produced in the model. The results for the temperature anomaly were taken at a longitude point of 65°N, and at the equator. The time axis represents the time integration of the model in Earth days.

In the Figure 4.2, it is possible to observe in the polar region of this temperature anomaly representation that the model reproduces qualitatively the cold "collar" in the middle atmosphere and a warm pole in the upper atmosphere.

The model implements a condensing cloud parameterisation which includes: condensation, evaporation and sedimentation of a mono-modal sulphuric acid cloud. The condensation and evaporation are two instantaneous processes, determined by the saturation vapour pressure (SVP) profile for acid sulphuric vapour. The sedimentation rates are determined by the pressure dependent viscosity of carbon dioxide, where is assumed that particles fall at their terminal Stoke velocity (Lee et al. (2009) and Lee et al. (2007)). Using this passive tracer scheme, large structures in the atmosphere very similar to those observed were found: the "Y" shape and reversed "C" shape features. The model includes also an ideal diurnal cycle parameterisation. The simple formulation perturbates the thermal relaxation field in a form of a "hot spot" that varies with the Sun's position, creating diurnal and semi-diurnal tides in the atmosphere, that contributes to the equatorward momentum transport, maintains the equatorial super-rotation in the model and produces a stronger global super-rotation.

A more complex boundary layer was tested in the model, a Monin-Obukhov boundary layer parameterisation, which was integrated with a realistic topography for Venus, but the results did not show any significant influence in the global mean circulation.

4.2 Simple Parameterisation

4.2.1 Thermal Forcing

Due to the difficulties of implementing an fully radiative transfer model optimised for fast computations suitable for a Venus GCM, the Oxford model uses a linear thermal relax-

ation instead (Lee, 2006). This parameterisation updates the temperatures at each point (λ-longitude, ϕ-latitude, p-pressure, t-time) of the GCM grid using,

$$\delta T_{rad}(\lambda, \phi, p, t) = -\frac{T(\lambda, \phi, p, t) - T_0(\phi, p)}{\tau}\delta t \tag{4.1}$$

where $T_0(\phi$,p) is the forcing thermal structure which gives the differences in temperature equator-to-pole, and τ is the constant of time in this formulation.

The form of the relaxation temperature is,

$$T_0(\phi, p) = T_{ref}(p) + T_1(p)(cos(\phi) - C). \tag{4.2}$$

In this equation we find T_{ref}(p) which is the reference temperature profile obtained from Seiff et al. (1980) and Seiff (1983), T_1(p) is a perturbation term that shape the equator-to-pole difference, and finally the constant C which is the integral of cos(ϕ) over the domain and has the value of $\frac{\pi}{4}$. The values of T_1(p) are chosen to give qualitatively the influence of the peak in absorption of solar insulation within the cloud deck (Tomasko et al., 1985). The values for the time constant used have been smaller than the values observed for the atmosphere of Venus to save computational time, and it is expected to have the same effect as large values. The true values for the relaxation time-scale are difficult to obtain due to the large value near the surface which could induce the observation of false values. The values for τ are 25 Earth days, decreasing slightly in the uppermost levels.

4.2.2 Boundary Layer Scheme

The surface boundary layer parameterisation used in the Venus GCM simulates the interaction between the surface and the atmosphere, and is based in a linear friction parameterisation which is fairly correct for Venus conditions (Lee, 2006). This simple formulation was constructed using,

$$\frac{d\vec{u}}{dt} = \frac{\vec{u}}{\tau_d}, \tag{4.3}$$

where τ_d is the relaxation time scale and $\vec{u}$ is the horizontal velocity vector at the lowest layer only (the velocity at the surface level is assumed to be equal to zero). The planet's surface is assumed to be flat, so the value for τ_d is the same at all the surface points, 32 Earth days, which using a relation between the relaxation period and the bulk transfer coefficients gives approximately the typical values for the Earth (Lee, 2006).

At the top three layers of the GCM, a sponge layer is included, with the same Rayleigh friction dumping the eddy components of the velocity field, to avoid the reflection of any wave in the numerically imposed rigid lid. The time constants were chosen from values between 100 and 0.01 Earth days, decreasing with altitude in the GCM grid.

CHAPTER 5

Research using OPUS-V

In a preliminary study of atmospheric transport on Venus, the SGCM has computed and obtained diagnostics from the surface to an altitude of around 90 km over complete annual and diurnal cycles, including simple representations of cloud formation and transport. Amongst other features, we investigate the possible existence of a meridional transport barrier in the atmosphere of Venus from the analysis of fields of potential vorticity (PV). There is also some evidence for cross-equatorial transport to be inhibited in the Earth's atmosphere (Chen et al. (1995) and Shuckburgh et al. (2001)).

We studied the nature of the flow by analysing the dominant terms in the meridional component of the equation of motion.

5.0.3 Atmospheric Transport

The transport barrier is a well known phenomenon in the Earth's atmosphere, and its mechanism is used to explain the isolation of the Antarctic ozone hole (Chen, 1994). These large-scale phenomena can be visualized from potential vorticity (PV) maps on isentropic surfaces or from the effective diffusivity of the cloud tracers' diagnostics. Those areas where the phenomena occur are related with strong PV gradients on the isentropic surface, where the Rossby-wave restoring mechanism suppresses Rossby-wave breaking. As a consequence, the parcel displacements take the form of reversible undulations, and the irreversible transport is inhibited.

The Venus Express observations have been indicating rapid changes in temperature, cloud morphology and structure, composition and zonal wind fields at altitudes of the lower mesosphere and upper troposphere at 50°-60° S in the atmosphere of Venus, which suggest a possible existence of a transport barrier (Titov et al. (2008) and Markiewicz et al. (2007)).

A preliminary study of the transport barrier in the Venus GCM was analysed using maps of the potential vorticity (PV) (McIntyre and Norton, 1990), to identify regions where the PV gradient on isentropic surfaces is relatively strong and the transport barrier is formed. The evidence for this phenomenon, which appears near the westward jets in Venus, is also observed in the Oxford Mars GCM (Figure 5.1).

In the present study, the amount of condensible tracer was initialised homogeneously on the GCM grid, at an instant after the spin-up of the model (41000 Earth's days). Sources and sinks of passive tracer were parametrized using the approach developed by Lee et al. (2009). The total mass of the tracers was set to give an approximate altitude of the cloud base at 50 km, which was distributed following the atmospheric conditions and the saturation vapour pressure profile of the sulphuric acid (see Figure 5.3).

Figure 5.2, shows four different instants separated by one Earth day and after a hundred Earth days following the initialisation of the passive tracer parameterisation. At this time

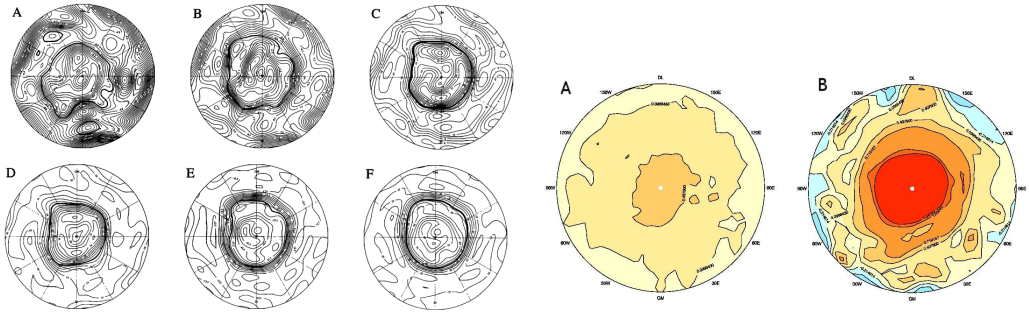

(a) Earth PV fields. (b) Mars PV fields.

Figure 5.1: These figures show some examples of the evidence of a mixing barrier which has been observed in the Earth **(a)** and Mars's atmosphere **(b)**. **(a)** is on the isentropic surfaces: (a) 350 K, (b) 375 K, (c) 400 K, (d) 425, (e) 450 K and (f) 500K; and the contour intervals are 0.4, 1, 1.5, 2.5 and 5 PVU. The units in **(b)** are in 100 PVU and the image is on the isentropic surfaces: (a) 300 K and (b) 500K.

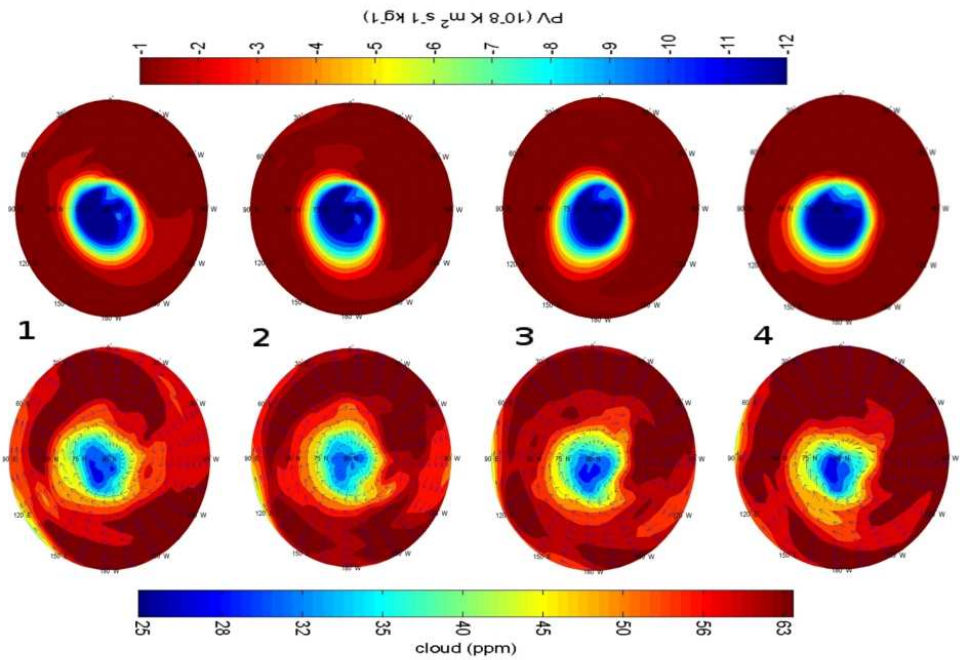

Figure 5.2: PV field on an isentropic surface (864 K) and the horizontal cloud distribution on a pressure surface (951 hPa) which corresponds roughly to the same altitude in the atmosphere, with one day of interval between each image.
Note:1 hPa=1 mba; PV units used: $10^{-8} Km^2 s^{-1}$

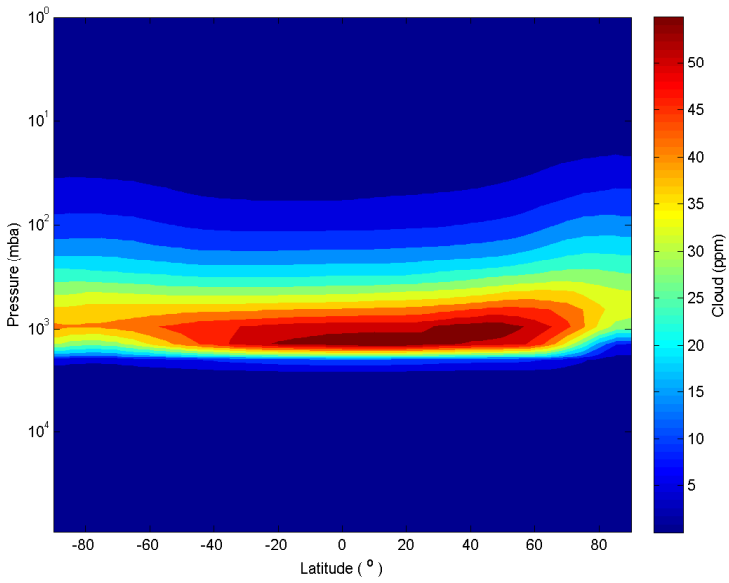

Figure 5.3: Zonal and time cloud liquid concentration. It was obtained after 41000 earth days in the GCM integration without diurnal forcing. The cloud variable was averaged over longitude and over time (40 days).

the tracers are well mixed in the atmosphere. The strong PV gradient creates an isolated area in the Polar region which is delimited by a possible transport barrier on that region. It is possible to verify on these results that this area corresponds to a region on the cloud maps, where in the centre is characterised by fewer amount of clouds compared to the outside. The altitude of the maps in the atmosphere for the clouds and PV, corresponds roughly to the same value of 1 bar. The four instants show qualitatively that the possible transport barrier has acted to inhibit the meridional transport. The small amount of clouds in the centre of the Polar Vortex is possibly due to an upwelling circulation. It is possible to see the effect of this upwelling circulation on the cloud deck on the Figure 5.3, where for high latitudes the tracers are transported to higher altitudes. The case studied may also be consistent with the mechanism where in the westward jets zone, the strong gradient of the PV is associated with a large Rossby wave restoring force, which inhibits meridional mixing at large scales. At small scales, the meridional shear acts to inhibit meridional mixing.

The transport barrier can be revealed more quantitatively by studies of effective diffusion in the atmosphere. To extend our study of atmospheric transport on Venus in the future, we will compute the effective diffusivity of cloud tracers and examine maps and profiles of diffusivity. The method that will be used has previously been applied to Earth's atmosphere e.g. by Haynes and Shuckburgh (2000) and Haynes and Shuckburgh (2000) and it was first introduced by Nakamura (1996). This new diagnostic which is a measure of the geometric structure of a tracer field, will allow us to identify transport barriers (as regions of small effective diffusivity - with simple geometric structure) and mixing regions (regions of large effective diffusivity - complex geometric structure) more easily.

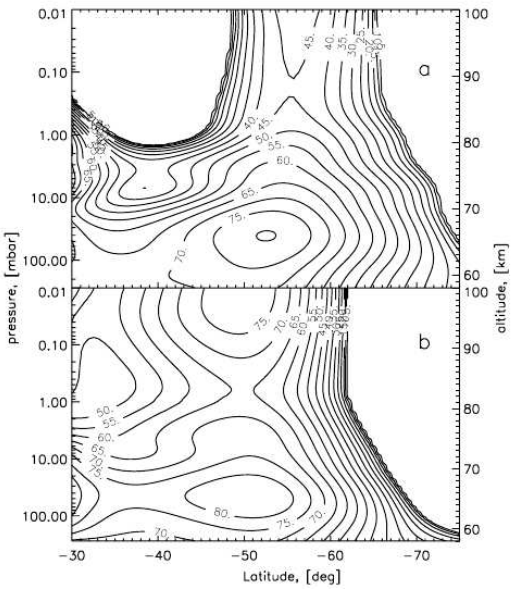

Figure 5.4: The two images show the contours of the zonal thermal wind speed (m/s) for two different local times: the top one is 18:00-20:00 and the other 03:00-05:00. These contours were obtained by Piccialli et al. (2008) assuming the cyclostrophic approximation at the mesosphere in Venus. The VIRTIS temperature retrivals were used.

The transport barrier that is evident in Mars and in the Earth, has an important role in determining the distribution of the clouds and consequently the dynamics of the atmosphere of Venus. Near the core of the jets, meridional tracer transport may be inhibited and forms a barrier that follows the dynamics of the waves.

5.0.4 Meridional Study of the Atmospheric Dynamics

From the meridional component of the equation of motion in a planetary atmosphere, we can obtain the thermal wind equation, assuming that the meridional gradient pressure term is in approximate balanced with the sum of the Coriolis and centrifugal terms,

$$2\Omega u \sin\phi + \frac{u^2 \tan\phi}{a} = -\frac{1}{\rho}\frac{\partial p}{\partial y}, \tag{5.1}$$

where ϕ is latitude, u the zonal wind, a the radius of the planet, p the pressure, ρ the density and ω the rotation rate of the planet. This equation can be simply written as a function of the temperature fields, assuming that we have an ideal gas. This equation may form the basis of a very useful tool to retrieve estimates of the atmospheric zonal wind from temperature measurements.

On Earth, which is a relatively rapidly rotating solid body, the geostrophic approximation is often assumed for large-scale atmospheric motions, where the pressure gradient term is approximately balanced with the Coriolis term. In the mesosphere of Venus, this

approximation fails because in those layers of the atmosphere we have strong winds overlying a slowly rotating planet. In this case, the cyclostrophic approximation may be used, in which the centrifugal term balances the gradient pressure term. Figure 5.4 shows a recent example of a derivation of the zonal wind using cyclostrophic approximation in the Venus mesosphere from VIRTIS temperature retrievals (Piccialli et al., 2008).

Where does this approximation give less accurate results? And what is the nature of those inaccuracies? These are some questions that a GCM which obtains a realistic and dynamically self-consistent representation of the circulation of the Venus' atmosphere, can help to answer.

In the present investigation we have studied the full zonally averaged meridional component of the equation of motion on a spherical planet of radius a and angular velocity Ω (see appendix A), in which we have analysed the contributions of different terms from the model's diagnostics. The aim was to elucidate the real nature of the atmosphere's zonal mean dynamics, especially at high latitudes, where cyclostrophic methods to retrieve the zonal winds seem to breakdown (i.e. they obtain winds close to or less than zero (Piccialli et al., 2008)) which seems to be in contradiction with other observations (e.g. the clear rotation of the double vortex structure (Piccioni et al., 2007)).

At the altitudes analysed in Figure 5.5, the results show that the zonal and time average of the equation of motion 5.1, is dominated mainly by three terms: the centrifugal acceleration, the geopotential gradient and the residual. The residual may be partly due to the variability of the flow with time, and seems to be related to the turbulent zone near the jets which may be dominated by eddy momentum fluxes.

More work can be done in this study, trying to find the real nature of the increasing magnitude of the residual at high latitudes, which seems to be more due to eddy momentum fluxes than numerical errors arising from the CFL filtering in the Polar regions.

The Figures 5.6 shows the evaluation of two of the main eddy terms obtained from the zonal and time average of the primitive equations (presented in appendix A), which do not have negligible magnitudes,

$$(a\cos\phi)^{-1}(\overline{v'^2}\cos\phi)_\phi, \tag{5.2a}$$

$$\overline{u'^2}a^{-1}\tan\phi, \tag{5.2b}$$

where the subscript denotes partial derivatives on the respective variable. Their influence are verified in the results showed in the Figures 5.7. The residual is reduced at high latitudes and at mid-latitudes at a pressure of 1 bar (Figure 5.7a).

The residual is not completely negligible at high latitudes, which is possibly related to the terms neglected or the CFL filtering, however for mid and low latitudes its magnitude is roughly zero. The work done until now, was just for two cases in the atmosphere, but more altitudes will be explored next, in order to try to understand the magnitude's variability of the eddy terms in space and time. These terms seem to be important in the Polar regions near the jets, however, leading to a breakdown of the cyclostrophic approximation (see Figure 5.7a in the South Polar region).

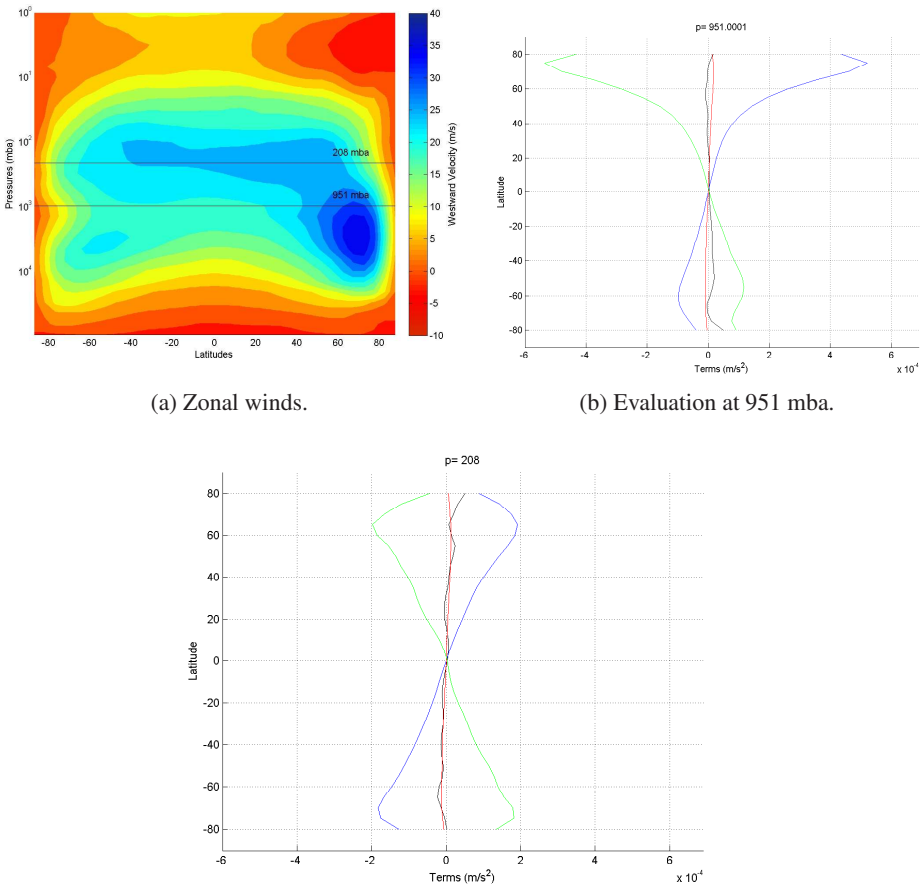

(a) Zonal winds.

(b) Evaluation at 951 mba.

(c) Evaluation at 208 mba.

Figure 5.5: The different colours represent each term of the meridional component of the equation of motion. They were obtained after 41000 earth days in the GCM integration without diurnal forcing, and afterwards over 150 days with diurnal forcing. Each variable v, w, u and Φ, was averaged over longitude and over time (40 days). The two lines on **(a)** show the altitudes where the plots **(b)** and **(c)** were evaluated. Note: Residual + $\frac{u^2 tan\phi}{a}$ + $u2\Omega sin\theta$ = $-\frac{1}{a}\frac{\partial\Phi}{\partial\theta}$;where θ is latitude and Ω is the rotation rate of the planet.

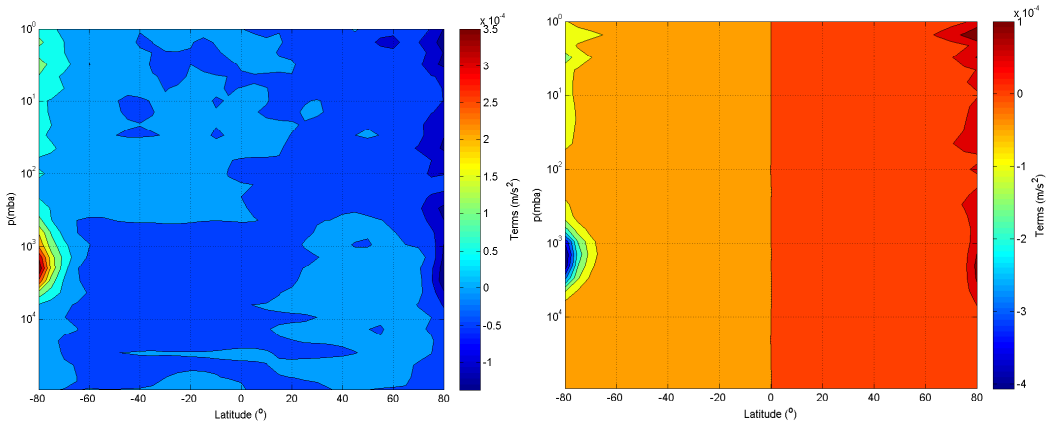

(a) Eddy forcing term: $(a\cos\phi)^{-1}(\overline{v'^2}\cos\phi)_\phi$.

(b) Eddy forcing term: $\overline{u'^2}a^{-1}\tan\phi$. .

Figure 5.6: Eddy terms obtained from the average done to the primitive equation in figure 5.5. The deduction of these terms are explained in the appendix A.

The next step will be to measure the physical causes for this increase in the residual at high latitudes, and perhaps to obtain a modified form of the cyclostrophic relation that could improve the methods to retrieve the zonal wind from the observed temperature fields. This new method has to take into account the eddy terms, which could perhaps be done using an eddy diffusion parametrization.

There is still work to do on the influence of these eddy forcing terms in the atmospheric circulation and it is also necessary to study more altitudes in the atmosphere.

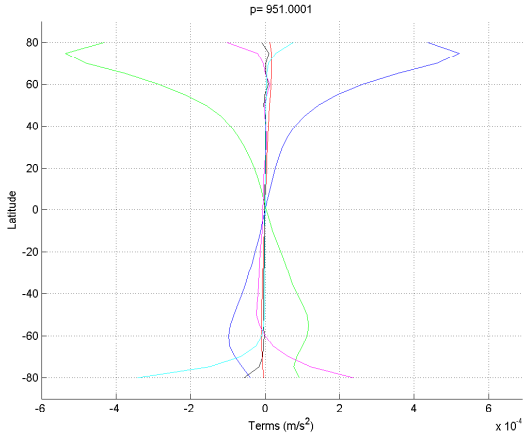

(a) Evaluation at 951 mba.

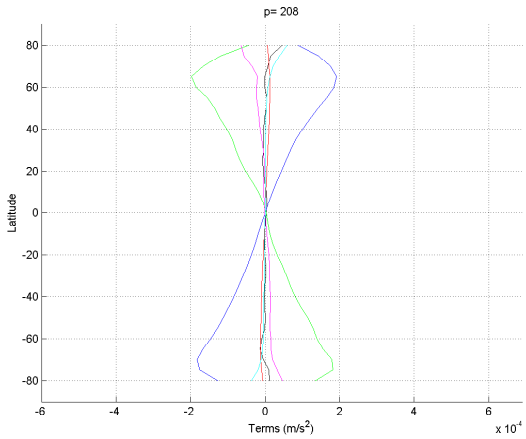

(b) Evaluation at 208 mba.

Figure 5.7: The different colours represent each term of the meridional component of the equation of motion. They were obtained after 4000 earth days in the GCM integration without diurnal forcing, and afterwards over 150 days with diurnal forcing. Each variable v, w, u and Φ, was averaged over longitude and over time (40 days). Note: Residual + $\frac{u^2 tan\phi}{a}$ + $u2\Omega sin\theta$ = $-\frac{1}{a}\frac{\partial\Phi}{\partial\theta}$- $(a\cos\phi)^{-1}(\overline{v'^2}\cos\phi)_\phi$ - $\overline{u'^2}a^{-1}\tan\phi$;where θ is latitude, Ω is the rotation rate of the planet and the primes mean the departure from the zonal mean.

CHAPTER 6

New Radiative Scheme on OPUS-V

Contents

In this work we adapt and extend the existing 3D time-dependent numerical circulation of Venus's atmosphere to include a new physically-based radiative transfer formulation in the infrared. This new parameterisation is based on the net exchange approach in Dufresne et al. (2005) and Eymet et al. (2009). Until now, the radiative scheme has only been studied for a single column in the GCM, at a zenith angle equal to 0°.

6.1 Shortwaves' Scheme

The vertical solar heating rates profile was computed using the Solar flux profiles obtained using a radiative transfer model from Crisp (1986). The model includes the expected sources of extinction in the mesosphere, and includes the absorption and scattering of CO_2, H_2O, SO_2, H_2SO_4 aerosols and an unidentified UV absorber as well (Crisp, 1986).

This parameterisation is expected to be improved by adapting a short-wave radiation parameterisation based on a general 2-stream Delta-Eddington code present in the HadAm3 model (Ingram et al., 2004) or adapting the one used in the Oxford Mars GCM (Forget et al., 1999).

6.2 Longwaves' Scheme

6.2.1 The Problem

Fast and accurate computations of the atmosphere's energy exchange via infrared radiation for long periods of integration, has been a challenging problem within the Venus GCM

community. Here we adapt the Net-Exchange parameterisation of thermal IR radiative transfer in Venus's atmosphere from Eymet et al. (2009) and Dufresne et al. (2005).

The implementation of a physically-based IR radiative representation on a Venus GCM, has some extra difficulties due to its particular atmosphere, which is mainly composed of CO_2 with a huge optical thickness and clouds with high single-scattering albedo in some important spectral ranges. The algorithm proposed in our research, is a simple code capable of rapidly computing the exchanges of IR radiative energy between different layers of the atmosphere, surface and space.

6.2.2 Net-Exchange Rate Matrix

The Net-Exchange Rate (NER) formalism adopted for the IR, is based on ideas originally proposed by Green (1967), and applied initially in a Venus GCM by Lebonnois et al. (2005). Its result is a matrix that corresponds to a vertical discretisation of n layers of the atmosphere plus the surface and the space. The definition of the NER (Ψ(i,j)) between two elements of the vertical discretisation (i and j) is the power emitted by j and absorbed by i, minus the inverse, the power emitted by i and absorbed by j. If Ψ(i,j) > 0, this means that the element i absorbs more than emits in the exchanges with j. The matrix Ψ(i,j) has properties of an antisymmetric matrix, Ψ(i,j) = - Ψ(j,i), and since the exchanges of energy within i are not permitted, all the elements of the matrix diagonal are zero. The amplitude of each Ψ(i,j) depends mainly on three properties:

- the difference of temperature between i and j;
- the local emission and absorption of i and j;
- the attenuation of radiation along the optical path between i and j.

6.2.3 Adaptation of the NER Formalim

The adaptation of the NER formalism to the GCM code has been done based on a simple parameterisation (Dufresne et al., 2005),

$$\Psi_{nb}(i,j) = \overline{\xi}_{nb}(i,j)(B_{nb}(j) - B_{nb}(i)). \tag{6.1}$$

The Net-Exchange Rates for each narrow wavelength band (Ψ_{nb}(i,j)) are evaluated from the difference in the Planck function at the mass weighted averaged temperatures for different layers, i and j, multiplied by an exchange factor $\overline{\xi}$(i,j) obtained with a complete radiative transfer model (KARINE) which depends on optical properties. Maintaining the atmospheric composition constant and assuming that variations in temperature do not affect the absorption and scattering cross sections, the values for $\overline{\xi}_{nb}(i,j)$ stay the same, which means that approximately $\Psi_{nb}(i,j)$ depends only on the temperature profile.

This simple parameterisation obeys to the reciprocity and energy conservation principles. Any upgrade to this parameterisation, as to include some sensitivity to clouds variations in composition or in structure, cannot violate any of these principles. One possible

extension is to include the sensitivity of the opacity to temperature variations which can be obtained from analytic results available in Eymet et al. (2005) for the upper atmosphere and, (in approximation), extended for all altitudes. This upgrade, contains the sensitivity of the opacity with temperature, was deduced from a linear expansion of the exchange factor around a reference temperature profile (VIRA's data). After that, the new formulation has to be adapted to be used in a GCM, fixing possible problems with the memory storage and violation principles, which can be done by linearising the Planck function as well, and studying the validity of the solutions.

6.2.4 KARINE

As said above, the exchange factor $\overline{\xi}$(i,j) is computed using a complete radiative transfer model that assumes a reference atmosphere with composition and structure constant in time, due to the difficulties to compute efficiently $\overline{\xi}$(i,j) in a GCM. The radiative transfer model KARINE, which is based on a Net-Exchange Monte-Carlo algorithm (Eymet, 2007), uses the gas and cloud spectra to produce $\overline{\xi}$(i,j) for 31 layers of the atmosphere (the vertical discretisation used in the Oxford Venus GCM) and a spectral range from 1.71 to 250μm.

The correlated-k coefficients for a particular atmospheric composition of CO_2, H_2O, S_2, CO, HDO, H_2S, HCl and HF, assumed to be uniform, were computed in Eymet (2007). Coupled with this data, the properties and distribution from an altitude of 47 to 70 km, of four different particles modes from a cloud model were included (Zasova et al., 2007). From these data KARINE code computed the net exchange factor $\overline{\xi}$(i,j) needed.

6.3 Results

6.3.1 IR Radiative Budget and Net-Exchange Rate matrix

The Figure 6.1 shows the first results of the NER matrix and the net radiative budget computed, already adapted for the vertical resolution of the Venus GCM, applied to the VIRA (Venus International Reference Atmosphere) temperature profile.

The NER matrix and the net radiative budget, Figure 6.1, show some interesting features regarding the interaction radiation-atmosphere. In the deep atmosphere, the net exchanges between layers are more relevant with their close neighbours, due to the strong opacity from the overlapping of gaseous absorption lines caused by high pressures. At wavelengths for which the gas of the atmosphere is quite transparent but not for the continuum absorption by cloud droplets, a warm peak in the cloud bottom is produced, being visible in the net radiative budget and in the long wings of the NER matrix plot. The backscattering affects the NERs below and above the clouds. The cloud deck from 47 km to 57 km, heats from the lower part and cools from the upper part where in the inside of the cloud the radiative exchanges are quite complex due to the importance of the scattering. Above the cloud, the atmosphere allows longer exchanges of energy than what is observed in the lower atmosphere due to the less intense effect of the pressure broadening. For these layers which are heated by the deep atmosphere, the exchanges with space are very important, resulting in its cooling. The space and the ground are continuous absorbers are settled

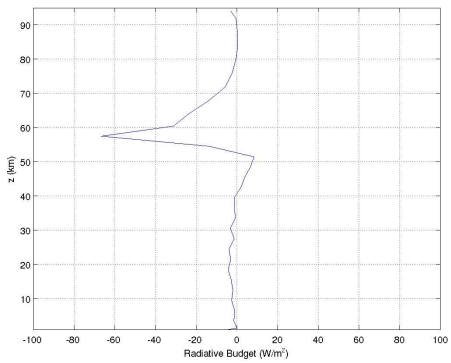

(a) Radiative Budget (W/m^2)

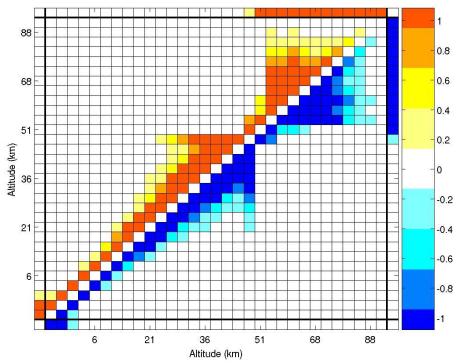

(b) Net Exchange Rate matrix (W/m^2)

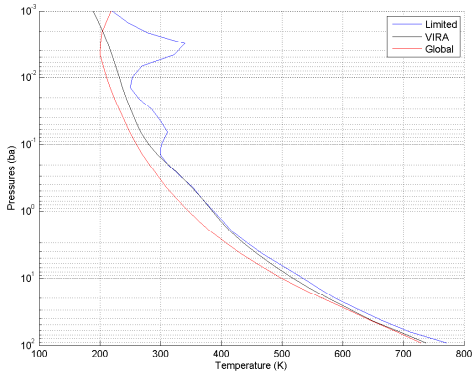

(c) Temperature (K)

Figure 6.1: **(a)** The initial radiative budget(W/m^2) as function of altitude. **(b)** The initial spectrally integrated Net Exchange Rate matrix. **(c)** Temperature profile after 20 Earth days of integration in the 1D GCM for the case of the limited area and 1500 days for the general configuration. In the last case the values were averaged over the last 50 Earth's days.
Note: There are 31 atmospheric layers plus the space (layer index 33) and the surface (layer index 1). These last two act as black bodies.

at a temperature of 3 K and 735 K respectively.

6.3.2 Vertical Temperature profile

To update the temperatures for each vertical layer, one needs to define the total radiative budget($\zeta(i)$) from the contribution of all narrow wavelength bands (nb),

$$\zeta(i) = \sum_{nb} \sum_{j=0}^{m+1} \Psi_{nb}(i,j), \tag{6.2}$$

where m is the number of atmospheric layers, plus the surface (j=0) and the space (j=m+1). The temperature was updated in each time step (δt) in a 1D vertical column in the GCM using the NER matrix.

$$T^{t+\delta t}(i) = T^{t}(i) + \frac{\zeta^{t}(i) \times \delta t}{m(i) \times C_p(i)}, \tag{6.3}$$

where m(i) and C_p(i) are the averaged mass and specific heat for each atmospheric layer. The radiative bugdget on this equation is the sum of the contribution of short and long-wavelength schemes.

Using the equations above, the temperature was updated after each timestep of 600 seconds for all the points of a column in our model. The need of accurate results and to fix some programming problems, the radiative code was implemented to evolve in one dimension for one column in the GCM grid. This implementation can be important for future tests and studies of other planet's atmospheres.

The idea to test the radiative code in just one column was tested using two different methods:

- The first method was based on Zuchowski (2009) codes, who used a limited area configuration applied to the 'Unified Model' codes, which are the basic of the OPUS-V. This code needs to have the boundary conditions of this area specified. In our tests, a 3x3 horizontal grid over 31 levels was used. The values for boundary conditions were taken from the results of the OPUS-V after the spin-up phase (40000 Earth's days of integration) for points near the equator, and the vertical profiles of the temperatures from the Venus International Reference Atmosphere (VIRA).

- In the second method, a general grid configuration was used, the same as in the OPUS-V, where the radiative code was defined to just run in a column near the equator. The atmosphere starts from the rest and with the same profile of temperature (VIRA) for all the columns in the GCM grid. The horizontal difusion and filtering were not included in these simulations.

For the first case, the limited area of 3x3, the boundary conditions constrains the dynamics of the column at the centre, causing problems of stability in the model when this

one has to adapt to a different heating and cooling rate profiles. The new radiative code forces the atmosphere in a different way than the newtonian cooling used to obtain the boundary values which does not change with time. This causes some problems in the code, it was only possible to have 20 days of integration until the model becoming unstable. The Figure 6.1c shows the differences between the profile obtained and the initial profile (VIRA temperature' profile) which starts to diverge mainly in the upper part of the vertical profile (above the clouds).

The other method (using a Global grid) integrates for 1500 days without becoming unstable. The values of the temperature profile for this case, Figure 6.1c, are below the VIRA's profile until a pressure of 2 mba. This difference can be reduced by calibrating the NER computations for future test cases and possibly improving the dynamical core to include the variations of the specific heat which is verified in the Venus' atmosphere (Seiff et al., 1985).

The new radiative scheme is capable of rapidly computing the energy exchange in the atmosphere. This simple parameterisation makes use of the output of a full radiative transfer model, which gives a more realistic picture of the energy exchange in the atmosphere than the Newtonian cooling approach.

CHAPTER 7

Preliminary Results from OPUS-T

Contents

We have developed a simplified atmospheric model to study the climate of Titan based in the OPUS-V (**O**xford **P**lanetary **U**nified **S**imulation model for **V**enus). The aim of this model is to study the dynamics of its atmosphere that shows some similarities to the dynamics of Venus. The simplicity of the parameterisations will roughly be the same, which can help to study their versatility to different conditions and perhaps improving them.

Some questions rise from the slow rotating bodies having super-rotating atmospheres like Venus and Titan, which is a very interesting result because it is counter intuitive if we think on the limit of no rotation. It is important to understand what are the mechanisms which are responsible for the super-rotation and if it is an inevitable condition for the slow rotation.

7.1 The Model

The OPUS-T (**O**xford **P**lanetary **U**nified **S**imulation model for **T**itan) was developed from an adaptation of the previous model for Venus (Lee et al., 2007), where the physical and dynamical conditions were changed to better suit Titan. Although its massive atmosphere, the main differences related with pressure and temperature profiles, and the existence of seasons in Titan, do not give a global dynamical picture too different from what is observed mainly for both upper atmospheres.

The Titan SGCM developed here is in a very early stage, where it was not possible to observe enough diagnostics to understand if the model is producing some of the Titan's meteorology or find possible errors in the model's code. For now, the model which starts from a rest atmosphere is still running in a spin-up phase.

7.2 Simple Parameterisations

The OPUS-T which was adapted from the OPUS-V, started from the Unified Model developed in the United Kingdom Meteorological Office (UKMO), as was said in the Venus section.

7.2.1 Basic Parameters

The present simple Titan GCM, used an unchanged boundary layer with a linear friction scheme and an adapted thermal forcing as well as the variables characteristic of its motion and physical characteristics (Table 2.1) and its resolution, 37x72 horizontal per 52 vertical levels covering 200 km (Table 7.1). The ellipticity of Titan's orbit around the Sun was neglected and it was assumed that its orbiting in synchronous around Saturn. Maintaining the same horizontal resolution and time step as the Venus model, we are still satisfying the CFL's (Courant-Friedrichs-Lewy) condition, which filters any zonal winds which are too fast comparing the wind speeds for that latitude orientation. As the Titan's radius (r_T) is less than the Venus radius, the running of the Titan model becomes more unstable (potential temperature and surface pressure appear negative in several points of the GCM grid), keeping the same time step (Δt), horizontal resolution ($\Delta\phi$) and the strength of the diffusion (K). These values should obey to the stability criterion,

$$\Delta t(\frac{4K}{{r_T}^2\Delta\phi^2})^j \leq 1, \tag{7.1}$$

where j is related with the order of diffusion, from the numerical eddy diffusion routine which filters the entire model domain (j=3, gives an order of diffusion equal to 6). This criterion limits the values of K that unsure a stable model, which are for all the altitudes less than the values used for Venus, once the other variables in the criterion remain unchanged.

7.2.2 Radiative Forcing

The thermal forcing (in the Venus research section) was adapted to include diurnal and seasonal forcing, where the inclination angle of the rotation axis with the ecliptic plane is around 27°. The vertical profile of the reference temperature for Titan (T_{ref}) is given in the Figure 2.11 (Lindal et al., 1983). As it was done for Venus, the time scales are less in general than the values obtained in the radiative transfer models. The values for τ are 8 Earth days, decreasing slightly in the uppermost levels. The vertical temperature perturbation profile, T_1(p), is given in the Table 7.1, where it was chosen to reflect the peak in absorption of the solar and thermal radiation obtained in McKay et al. (1989).

Two versions of the Titan SGCM were developed, with and without diurnal forcing. The one without diurnal forcing, uses a thermal forcing parameterisarion similar to the one used for Venus. In this case, the temperatures of all points of the GCM grid relax to a zonal averaged temperature profile, that depends on the seasonal variations given by the solar declination angle (see Figure 7.1),

Level	Altitude (km)	Pressure (mba)	T_{ref} (K)	T_1 (K)	τ (Earth Days)	K ($\times 10^8$)
1	1.0	1421.48	92.6	2.000	8.0	5.00
2	2.0	1350.40	91.2	2.000	8.0	5.00
3	4.0	1216.28	88.9	2.000	8.0	5.00
4	8.0	980.98	85.3	2.000	8.0	5.00
5	12.0	785.43	82.2	2.000	8.0	5.00
6	16.0	624.87	79.5	2.000	8.0	5.00
7	20.0	494.04	77.0	2.001	8.0	5.00
8	24.0	388.68	75.1	2.014	8.0	5.00
9	28.0	304.45	73.5	2.083	8.0	5.00
10	32.0	237.68	72.3	2.313	8.0	5.00
11	36.0	185.22	71.7	2.855	8.0	5.00
12	40.0	144.26	71.2	2.843	8.0	5.00
13	44.0	112.40	71.4	4.522	8.0	5.00
14	48.0	87.75	71.6	7.200	8.0	5.00
15	52.0	68.67	72.2	9.297	8.0	5.00
16	56.0	53.97	73.6	11.370	8.0	5.00
17	60.0	42.78	77.5	13.196	8.0	5.00
18	64.0	34.48	85.4	14.606	8.0	5.00
19	68.0	28.54	99.1	15.510	8.0	5.00
20	72.0	24.20	110.8	15.892	8.0	5.00
21	76.0	20.81	118.4	15.794	8.0	5.00
22	80.0	18.06	124.4	15.298	8.0	5.00
23	84.0	15.79	130.4	14.498	8.0	5.00
24	88.0	13.88	135.1	13.498	8.0	5.00
25	92.0	12.25	137.1	12.374	8.0	5.00
26	96.0	10.84	140.6	11.213	8.0	5.00
27	100.0	9.62	143.1	10.067	8.0	5.00
28	104.0	8.56	145.6	8.978	8.0	5.00
29	108.0	7.63	147.8	7.792	8.0	5.00
30	112.0	6.81	149.2	7.064	8.0	5.00
31	116.0	6.09	150.7	6.259	8.0	5.00
32	120.0	5.46	152.1	5.556	8.0	5.00
33	124.0	4.89	154.0	4.952	8.0	5.00
34	128.0	4.40	156.1	4.436	8.0	5.00
35	132.0	3.96	157.8	4.001	8.0	5.00
36	136.0	3.57	159.0	3.637	8.0	5.00
37	140.0	3.22	160.1	3.334	8.0	5.00
38	144.0	2.91	161.5	3.084	8.0	5.00
39	148.0	2.63	162.3	2.878	8.0	5.00
40	152.0	2.38	163.1	2.710	8.0	5.00
41	156.0	2.15	164.5	2.572	8.0	5.00
42	160.0	1.95	165.3	2.461	8.0	5.00

Level	Altitude (km)	Pressure (mba)	T_{ref} (K)	T_1 (K)	τ (Earth Days)	K ($\times 10^8$)
43	164.0	1.77	165.7	2.370	8.0	5.00
44	168.0	1.61	166.9	2.297	8.0	5.00
45	172.0	1.46	167.0	2.239	8.0	5.00
46	176.0	1.33	167.2	2.191	8.0	5.10
47	180.0	1.20	167.2	2.171	8.0	5.15
48	184.0	1.10	167.4	2.122	8.0	5.30
49	188.0	1.00	167.9	2.098	8.0	5.60
50	192.0	0.91	168.3	2.078	8.0	6.00
51	196.0	0.83	168.8	2.063	6.0	6.50
52	200.0	0.75	169.4	2.050	5.0	7.00

Table 7.1: Values used in the Titan GCM.

$$\delta T_{rad}(\lambda, \phi, p, t) = -\frac{T(\lambda, \phi, p, t) - T_0(\phi, p)}{\tau}\delta t, \tag{7.2}$$

$$T_0(\phi, p) = T_{ref}(p) + T_1(p)(cos(\theta - \delta) - C) \tag{7.3}$$

where C is equal to $\frac{\pi \cos\delta}{4}$, which is the integral of cos($\theta - \delta$) over the domain, and δ is the solar declination angle. The values for δ are simplified, they are assumed to vary sinusoidally between the maximum value 27° and the minimum -27°.

The diurnal and seasonal forcings are simulated by a very simple non realistic horizontal perturbation ("hotspot"), that varies its longitude and latitude with the Sun's position. The horizontal temperature perturbation is given by the cosine of the polar zenith angle (θ_s),

$$cos(\theta_s) = sin(\phi)sin(\delta) + cos(\phi)cos(\delta)cos(H_a), \tag{7.4}$$

where H_a is the local hour of the Sun. The Figure 7.2 shows one instant of this hotspot.

This simple parameterisation for the thermal forcing using a simple diurnal forcing in Titan, can be written in the extended form using the notation from the Venus research section,

$$\delta T_{rad}(\lambda, \phi, p, t) = -\frac{T(\lambda, \phi, p, t) - {T_0}^d(\lambda, \phi, p)}{\tau}\delta t, \tag{7.5}$$

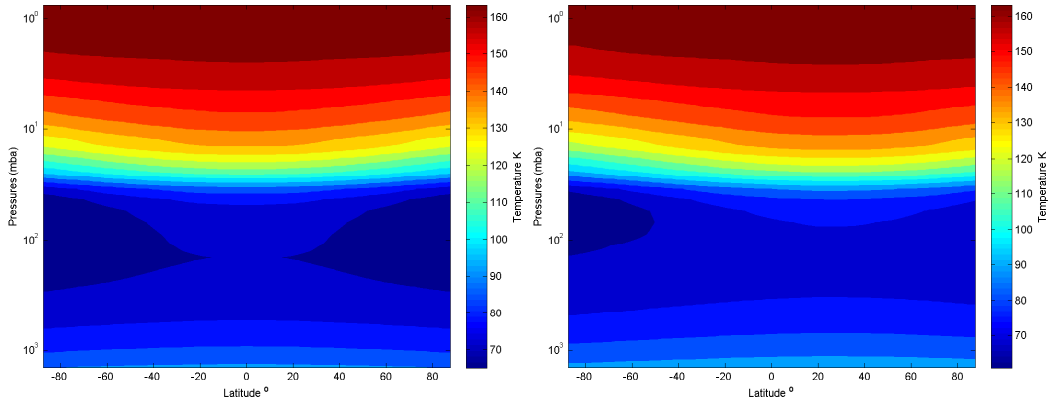

(a) Zonal averaged temperature field (δ = 0) (b) Zonal averaged temperature field (δ = 27)

Figure 7.1: Zonal temperature fields for two different declination angles, **a** δ = 0 (one equinox) and **b** δ = 27 (North summer solstice).

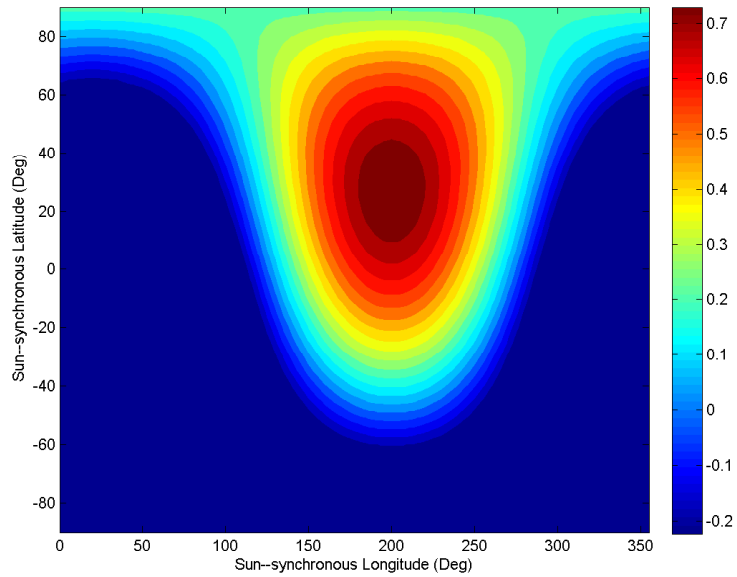

Figure 7.2: Horizontal temperature perturbation, "hotspot", used for diurnal and seasonal forcing. This perturbation varies its position with the zenith angle (θ_s). The image shows the values of $cos(\theta_s) - \frac{\cos\delta}{4}$ for a South winter season.

$$T_0{}^d(\lambda, \phi, p) = T_{ref}(p) + T_1(p)(cos(\theta_s) - C_d), \tag{7.6}$$

where C_d is $\frac{\cos\delta}{4}$, which is the integral of $\cos(\theta_s)$ over the domain ($cos(\theta_s)$ in the night side of the planet, is forced to be zero). The diurnal and seasonal forcings implemented have a very simple form, and their influence on the dynamics of the atmosphere will be studied in future work.

7.3 Spin-up Phase

As said above, the model is currently integrating on its spin-up phase, with some possible problems in the code to be corrected in the future. This first simulation of the SGCM for Titan with seasons has now roughly integrated for 3000 Earth's days (for both versions - with/without diurnal forcing). The simulation started from a state of rest with no horizontal temperature variations and using the vertical profile from Lindal et al. (1983).

From Figure 7.3 it is expected that the model is still in the spin-up phase, where the two Eastward winds profiles show an increase of the magnitude of the winds, mainly for the last days. Figure 7.4 shows some of the diagnostics obtained in this phase which is expected to be longer than the Venus simple model (23000 Earth's days), with one of the reasons being the increase of the vertical discretisation to 52 levels.

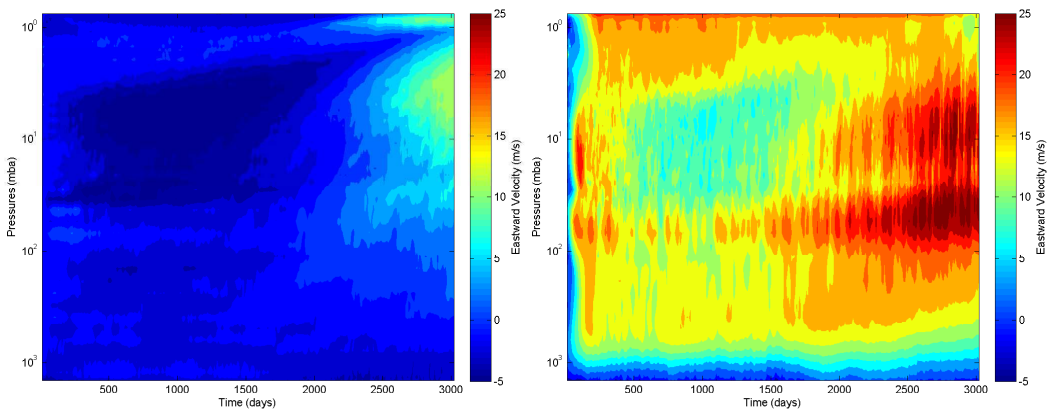

(a) Eastward winds (m/s) (At Equator) (b) Eastward winds (m/s) (At 67.5 ^{o} of Latitude)

Figure 7.3: The two figures show the Eastward wind speeds from two different positions: Equator **(a)** and at 67.5 ^{o} of latitude **(b)**.

In Hourdin et al. (1995), a complete radiative transfer model from McKay et al. (1989) was used, the simulation performed the spin-up phase over 23 Titan years (1 Titan year = 10752.17 Earth days). It is expected that the model will reach a stable-state regime earlier than a Full GCM, due to the shorter relaxation period used in the newtonian cooling than the values obtained in a realistic radiative transfer model.

There are several methods that can be used in the future to study this phase and predict its end. The method used in Hourdin et al. (1995), where they obtained a strong super-rotation after a long spin-up phase, was evaluated with the planetary averaged dimensionless angular momentum (μ) which is an index of super-rotation and is defined by:

$$\mu = \frac{a\cos\phi(u + a\Omega\cos\phi)}{\frac{2}{3a^2\Omega}}, \tag{7.7}$$

where a is the planet radius, ϕ is latitude, Ω is the rotation rate of the solid body and u is the zonal velocity. The equation is the ratio of the specific angular momentum over the mean specific angular momentum of the atmosphere at rest. Other method which was used in Lee (2006), computed the globally integrated kinetic energy, which is defined as,

$$E_k = \int \frac{(u^2 + v^2 + w^2)a^2\cos\phi}{g} d\phi d\lambda dp, \tag{7.8}$$

where u, v and w are the velocity components, ϕ and λ are the latitude and the longitude, p the pressure and g the gravitational acceleration.

These two variables are expected to increase during the spin-up phase. After that period the model enters a stable-state and these two variables stop their monotonic increase becoming, in average, constant and possibly with oscillations due to the seasons effect on the atmosphere's circulation.

The Figures 7.4 show two versions of the SGCM for Titan: the model run with and without diurnal forcing. In both versions, Figures 7.4a and 7.4b show an atmosphere with zonal winds mainly in the Eastward direction. The effects of the diurnal forcing seem to reduce the magnitude of the jets, and its large influence on the circulation is due to the short timescale used on this version of the model to simulate diurnal variations (see Table 7.1).

Although the fact that we are still in the spin-up phase, it is already possible to verify in the results obtained, the formation of strong winds in the equatorial zone in the middle atmosphere of our simulations. These diagnostics need to be studied more carefully, as well as the Northward winds diagnostics which show two Hadley cells (see Figure 7.4c) in the upper atmosphere and the temperature diagnostics where it is possible to verify the existence of the warm pole phenomenon (see Figure 7.4d). It is premature to have more conclusions or more detail studies about these recent results because they are not in the steady-state regime, that is more closely related with Titan atmosphere's conditions.

Note: Our simulations used a constant value for C equal to $\frac{\pi}{4}$, in the relaxation temperature parameterisation, corresponding to an equinox's value. If we integrate the C used here and the C showed in the parameterisation without diurnal forcing, C = $\frac{\pi\cos\delta}{4}$, in order into account the variation in the declination angle over a Titan year, we can obtain the difference of these two funtions after one year of integration. The result show that for the value

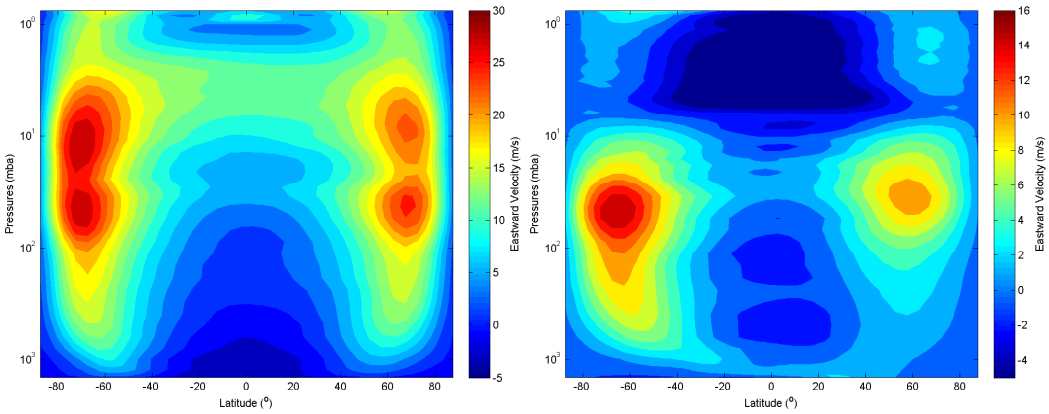

(a) Eastward Velocity (m/s) without diurnal forcing

(b) Eastward Velocity (m/s) with diurnal forcing

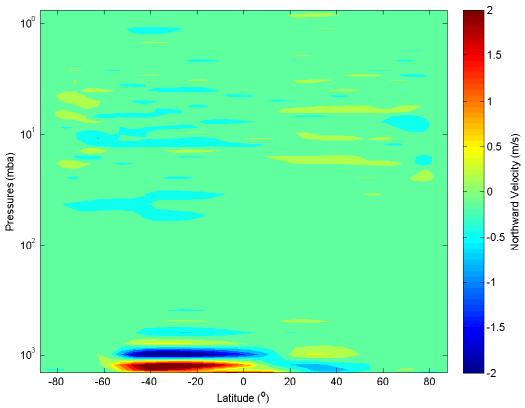

(c) Northward Velocity (m/s) without diurnal forcing

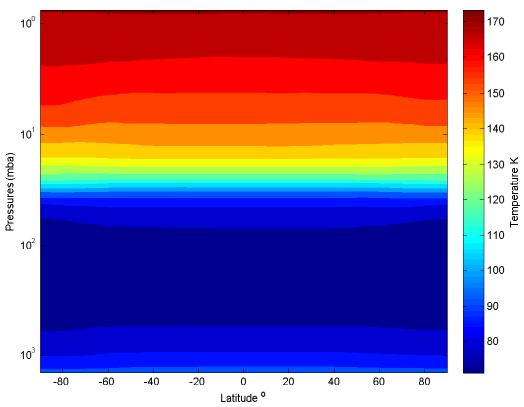

(d) Temperature (K) without diurnal forcing

Figure 7.4: Prognostic variable diagnostics after 50 days of zonal average from the OPUS-T and roughly 3000 days of integration, with and without diurnal forcing. **(a)** Westward wind speed (m/s) without diurnal forcing. **(a)** Westward wind speed (m/s) with diurnal forcing.**(c)** Northward wind speed (m/s). **(d)** Temperature. The results were obtained during the southern spring equinox.

of C used in the parameterisation without diurnal forcing, the global integration is roughly 2 times smaller than the integration using the constant value. Due to this assumption, that was corrected recently, the SGCM for Titan obtained a vertical global temperature profile that is globally below the reference temperature profile (see Table 7.1).

CHAPTER 8

Conclusions and Future Work

Contents

8.1 Conclusions

As it will be explained in the next section, there remains a lot of work to be done concerning the improved Full Venus GCM or in the simplified Titan's version to study new circulations in the simulated atmospheres.

In the Full Venus GCM, the new radiative scheme needs a calibration and more test cases to try to find possible errors in the code. For now, the results from this parameterisation seems to be close of the accuracy needed, that could be improved studying carefully the vertical composition of the atmosphere that we are using in KARINE, by doing comparative test cases with the advanced radiative transfer model NEMESIS (Irwin et al., 2008). The time spend in computation, needs to be improved for a future implementation in a global atmosphere, and this problem can be solved by changing the Full GCM studies to a faster computer.

The transport barriers research and the residual calculation from the meridional flow equation needs to be explored, because they show interesting results that were never studied from this point of view before, in the Venus GCM community. The clouds distribution in the polar Vortex due to the PV barrier and the residual's study could be compared with a future global dynamical picture of the atmosphere, obtained after the implementation of the new radiative scheme.

The Titan GCM seems to be evolving in the right direction but still in a too early stage to obtain relevant conclusions. It is expected that the model for Titan will stabilise before the 23 Titan years obtained in Hourdin et al. (1995). In that work they used a radiative transfer model that obtained larger values for the radiative timescales than the values fixed in our model. The model still does not show the wind pattern with the magnitude and orientation which has been obtaining by more complex models (prograde winds with a maximum magnitude of 100 ms^{-1} in the stratosphere). The end of this phase will be studied more carefully in future diagnostics, for example, the evolution of the planetary averaged dimensionless angular momentum or the kinetic energy of the global atmosphere

as it was pointed in Chapter 7. These quantities after the spin-up phase are expected to have a stable oscillation, due to seasons, over time.

8.2 Future Work

My future plan of work will be mainly to continue to improve and extend the existing OPUS-V in a more full GCM version and built a simplified GCM for Titan capable of reproducing qualitatively the main dynamic features of its atmosphere.

After an initial familiarisation with the Oxford SGCM for Venus and the new radiation scheme, the implementation needs to be tested in simulations in a more accurate global GCM. A further step will be to recalibrate and extend this scheme based on new computations of radiative transfer on Venus in the presence of clouds, using 1D advanced models previously developed in Oxford - NEMESIS (Irwin et al., 2008). Introducing a radiative transfer parameterisation for the short-waves will give us more flexibility, by making it easier to adapt to different conditions of the atmosphere. The GCM does not yet include a interface between the existing cloud parameterization and the radiation scheme, which from the prediction of the cloud locations and density would improve the accuracy of the radiative scheme results.

Other parameterisation schemes can also be included in our Venus GCM: boundary layer turbulence and topographic surface, and gravity wave drag. These schemes can be adapted from the UK-French Mars GCM (Forget et al., 1999). The thermal relaxation will continue to be subject to study and the data set for temperatures of reference will be updated, as well as to include more accurate equator-to-pole perturbations and thermal tide amplitudes based on VIRTIS data.

The dynamical core needs an upgrade to include variations of the specific heat C_p in the atmosphere of Venus, because the observations suggest important variations, from 738 JKg$^{-1}K^{-1}$ at 100 km altitude to 1181 JKg$^{-1}K^{-1}$ close to the surface (Seiff et al., 1985). These variations imply that a different way of evaluating the potential temperature is needed, since the adiabatic lapse rates will change for the whole atmosphere. This implementations will be based on the simple formulation available in Lebonnois et al. (2009).

Further development and validation of GCM simulations: diagnostic computations of eddy statistics, model climatology, clouds and heat and momentum transports. Sensitivity studies to topography, clouds and other parameters will be done to understand their influence in the atmospheric circulation.

In the observational side, it will be important to validate and verify the simulation using data from Venus Express, in particular the VIRTIS instrument and visual and UV imaging. I am also engaged with an upcoming international model inter-comparison exercise for Venus, being organised by the International Space Science Institute in Bern. The aim of this project is to study the influence of use different dynamical cores used in different Venus GCMs that use similar physical parameterizations. It will be possible as well to study the role of these parameterization for different test cases.

Titan GCM is in a very early stage and the parameterisation needs to be calibrated and studied more carefully, to correct and avoid some possible errors from the Venus GCM

Oct. 2009 - Dec. 2009	. Identification of test cases and reference computations using NEMESIS. . Calibration and implementation of the radiative code into Full GCM. . Spin-up Titan SGCM atmosphere to super-rotation and explore the influence of seasonal variations.
Oct. 2009 - Mid 2010	. Test simulations in the Venus Full GCM. . Implementation of other parametrisation schemes into Venus Full GCM. . Completion of the first reference GCM simulations for initial comparison with Venus Express data and Titan Cassini data.
Mid 2010 - Late 2010	. Further development and validation of GCM simulations. . Diagnostic computations of eddy statistics, model climatology, clouds and heat and momentum transports on Titan and Venus GCMs. . Sensitivity studies to topography, clouds and other parameters on Titan and Venus GCMs.
Late 2010 - Mid 2011	Completion of comparison studies.
Mid 2011 -	Writing thesis.

Table 8.1: Future work timeline

adaptation. Afterwards, the diagnostics will be computed for the model, validating and comparing with data from Cassini. The study of Titan GCM can offer new tools to learn more about the mechanism that creates the super-rotating atmosphere. Other phenomena to be studied in the model and compared with observational results (Teanby et al., 2008), is the possible existence of a transport barrier from the PV fields, as was done for Venus (see Chapter 5).

8.3 Approximate Timeline

It is always difficult to timeline the work that depends on the development of a numerical model, however, a suggested plan of work for the next three years is in Table 8.1.

Further Activities

My first year in Oxford has been a good experience, where I had the pleasure of study and work in a productive and dynamic research group complemented by the graduate lectures.

I had the opportunity to attend some conferences like: ESLAB, UK planetary forum and specially the Raymond Hide work celebration meeting. These meetings gave me a broad perspective of the work that has been done in planetary sciences, and the chance to meet and discuss with people who are working in my research area.

The oral presentations in my research group's meeting and the poster in the ESLAB conference were important in the way that I could improve my presentation skills. I had the opportunity to attend the super computing lectures as well, the maths works seminars where I learned more about the Matlab programming and Linux commands.

Last, but not the least, I attended the Academic Writing course in the Language Center, by the tutor Maggie Charles, which improved my writing skills for a more consistent writing, organised and with fewer grammatical errors.

Acknowledgements

I thank my supervisors for the motivating ideas, suggestions and guidance. I acknowledge financial support from FCT - Fundação para a Ciência e a Tecnologia (Portugal).

APPENDIX A

Basic Equations

The basic equations of atmospheric motion are called primitive equations. These set of nonlinear differential equations govern a wide variety of fluid motions and is the basis of the construction of most atmospheric and oceanic models.

A.1 Primitive Equations

The primitive equations represent the fundamental equations of motion in a rotating frame for an atmosphere. These equations are used not in their most general form, but there are several simplifications mainly based on scale analysis of each term of the equations which is usually done. Some of those procedures are usually about the distances from the centre of the Earth to any point of the atmosphere which is replaced by the mean radius, the hydrostatic balance replaces the vertical momentum, and the Coriolis force associated with the horizontal component of the Earth's rotation vector is neglected. The primitive equations using z as the vertical coordinate are,

$$\frac{Du}{Dt} - \left(f + \frac{u\tan\phi}{a}\right)v + \frac{\Phi_\lambda}{a\cos\phi} = X, \tag{A.1a}$$

$$\frac{Dv}{Dt} - \left(f + \frac{u\tan\phi}{a}\right)u + \frac{\Phi_\phi}{a} = Y, \tag{A.1b}$$

$$\Phi_z = H^{-1}R\theta e^{-\frac{kz}{H}}, \tag{A.1c}$$

$$\frac{[u_\lambda + (v\cos\phi)_\phi]}{a\cos} + \frac{(\rho_0 w)_z}{\rho_0} = 0, \tag{A.1d}$$

$$\frac{D\theta}{Dt} = Q, \tag{A.1e}$$

where the first two equations represent the momentum balanced in zonal and meridional directions, the third equation the hydrostatic balance, followed by the continuity of mass, and a thermodynamic relation between diabatic heating (Q) and the material derivative of the potential temperature (θ). Regarding the variable and parameters: (u,v,w) are the velocity components, (λ, ϕ) the horizontal components (longitude, latitude), f is the Coriolis parameter, X and Y are two horizontal components of some nonconservative mechanical forcing and ρ_0 the basic density.

A.2 The Eulerian-Mean Equations

In this section we apply an Eulerian mean to the equations A.1. This transformation on the equations is defined as an average over λ (longitude) fixing ϕ, t and z, for each term of the equations. The zonal average of each dependent variables is defined as the following example for zonal velocity,

$$\bar{u}(\phi, z, t) = (2\pi)^{-1} \int_0^{2\pi} u(\lambda, \phi, z, t)\, d\lambda. \tag{A.2}$$

To avoid lose information about the flow motion regarding the interaction of the mean flow with disturbances, we defined velocity components as,

$$u'(\lambda, \phi, z, t) = u - \bar{u}. \tag{A.3}$$

Applying this transformation to the equations A.1, we obtain the following set of primitive equations for the Eulerian-mean flow,

$$\begin{aligned} \bar{u}_t + \bar{v}[(a\cos\phi)^{-1}(\bar{u}\cos\phi)_\phi - f] + \bar{w}\bar{u}_z - \bar{X} \\ = -(a\cos^2\phi)^{-1}(\overline{v'u'}\cos^2\phi)_\phi - \rho_0^{-1}(\rho_0\overline{w'u'})_z, \end{aligned} \tag{A.4a}$$

$$\begin{aligned} \bar{v}_t + \bar{u}[\bar{u}a^{-1}\tan\phi + f] + a^{-1}\bar{v}\bar{v}_\phi + \bar{w}\bar{v}_z + a^{-1}\bar{\Phi}_\phi - \bar{Y} \\ = -(a\cos\phi)^{-1}(\overline{v'^2}\cos\phi)_\phi - \rho_0^{-1}(\rho_0\overline{w'v'})_z - \overline{u'^2}a^{-1}\tan\phi, \end{aligned} \tag{A.4b}$$

$$\bar{\Phi}_t - H^{-1}R\bar{\theta}e^{-\frac{kz}{H}} = 0, \tag{A.4c}$$

$$(a\cos\phi)^{-1}(\bar{v}\cos\phi)_\phi + \rho_0^{-1}(\rho_0\bar{w})_z = 0, \tag{A.4d}$$

$$\begin{aligned} \bar{\theta}_t + a^{-1}\bar{v}\bar{\theta}_\phi + \bar{w}\bar{\theta}_z - \bar{Q} \\ = -(a\cos\phi)^{-1}(\overline{v'\theta'}\cos\phi)_\phi - \rho_0^{-1}(\rho_0\overline{w'\theta'})_z, \end{aligned} \tag{A.4e}$$

where the subscript means partial derivatives on the respective variable, and the quadratic functions of disturbances variables, which were written in the right side of the equation, are the "rectified eddy-forcing" terms (Andrews et al., 1987). The functions of disturbances variables of lower order were neglected.

Bibliography

F. W. Taylor, Venus before Venus Express, PlanSS54 (2006) 1249–1262. v, 10, 13, 14, 15

C. Lee, Modelling of the Atmosphere of Venus, Ph.D. thesis, PhD Thesis, Oxford University (2006). v, vii, 3, 9, 12, 13, 27, 28, 30, 51

S. K. Atreya, Atmospheres and Ionospheres of the Outer Planets and their Satellites, 1986. vii, 18, 20

C. Lee, S. R. Lewis, P. L. Read, A bulk cloud parameterization in a Venus General Circulation Model, in Prep. 2, 29, 31

P. J. Gierasch, Meridional circulation and the maintenance of the Venus atmospheric rotation, Journal of Atmospheric Sciences 32 (1975) 1038–1044. 2, 14, 24

W. B. Rossow, G. P. Williams, Large-scale motion in the Venus stratosphere, Journal of Atmospheric Sciences 36 (1979) 377–389. 2, 14

C. Lee, S. R. Lewis, P. L. Read, Superrotation in a Venus general circulation model, Journal of Geophysical Research (Planets) 112 (E11) (2007) 4–+. 3, 13, 24, 27, 29, 45

R. M. Goldstein, Symposium on Radar and Radiometric Observations of Venus during the 1962 Conjunction: Venus characteristics by earth-based radar, Astron. J.69 (1964) 12–+. 6

R. L. Carpenter, Symposium on Radar and Radiometric Observations of Venus during the 1962 Conjunction: Study of Venus by CW radar, Astron. J.69 (1964) 2–+. 6

A. C. M. Correia, J. Laskar, The four final rotation states of Venus, Nature411 (2001) 767–770. 6

D. R. Williams, Venus fact sheet: National space science data center, http://nssdc.gsfc.nasa.gov/planetary/factsheet/venusfact.html. 9, 27

D. R. Williams, Earth fact sheet: National space science data center, http://nssdc.gsfc.nasa.gov/planetary/factsheet/earthfact.html. 9

A. Coustenis, F. Taylor, Titan : the earth-like moon, 1999. 9, 16

M. Allison, L. D. Travis, The Jovian Atmospheres, NASA Conference Publication 2441, New York. 9

R. W. Carlson, K. H. Baines, L. W. Kamp, P. R. Weissman, W. D. Smythe, A. C. Ocampo, T. V. Johnson, D. L. Matson, J. B. Pollack, D. Grinspoon, Galileo infrared imaging spectroscopy measurements at Venus, Science 253 (1991) 1541–1548. 11

D. Crisp, Greenhouse Effect and Radiative Balance on Earth and Venus, Presented in: 4th Meeting of Venus Exploration Analysis Group. 12

A. Seiff, D. B. Kirk, R. E. Young, R. C. Blanchard, J. T. Findlay, G. M. Kelly, S. C. Sommer, Measurements of thermal structure and thermal contrasts in the atmosphere of Venus and related dynamical observations - Results from the four Pioneer Venus probes, J. Geophys. Res.85 (1980) 7903–7933. 12, 13, 27, 30

J. B. Pollack, R. Young, Calculations of the radiative and dynamical state of the Venus atmosphere, Journal of Atmospheric Sciences 32 (1975) 1025–1037. 12

P. J. Gierasch, R. M. Goody, R. E. Young, D. Crisp, C. Edwards, R. Kahn, D. Rider, A. del Genio, R. Greeley, A. Hou, C. B. Leovy, D. McCleese, M. Newman, The General Circulation of the Venus Atmosphere: an Assessment, in: S. W. Bougher, D. M. Hunten, R. J. Philips (Eds.), Venus II: Geology, Geophysics, Atmosphere, and Solar Wind Environment, 1997, pp. 459–+. 12

S. W. Bougher, M. J. Alexander, H. G. Mayr, Upper Atmosphere Dynamics: Global Circulation and Gravity Waves, in: S. W. Bougher, D. M. Hunten, R. J. Philips (Eds.), Venus II: Geology, Geophysics, Atmosphere, and Solar Wind Environment, 1997, pp. 259–+. 12

C. B. Leovy, Rotation of the upper atmosphere of Venus., Journal of Atmospheric Sciences 30 (1973) 1218–1220. 14

S. B. Fels, R. S. Lindzen, The Interaction of Thermally Excited Gravity Waves with Mean Flows, Geophysical and Astrophysical Fluid Dynamics 6 (1974) 149–191. 14

T. Gold, S. Soter, Atmospheric Tides and the 4-Day Circulation on Venus, Icarus 14 (1971) 16–+. 14

G. Piccioni, P. Drossart, A. Sanchez-Lavega, R. Hueso, F. W. Taylor, C. F. Wilson, D. Grassi, L. Zasova, M. Moriconi, A. Adriani, S. Lebonnois, A. Coradini, B. Bézard, F. Angrilli, G. Arnold, K. H. Baines, G. Bellucci, J. Benkhoff, J. P. Bibring, A. Blanco, M. I. Blecka, R. W. Carlson, A. di Lellis, T. Encrenaz, S. Erard, S. Fonti, V. Formisano, T. Fouchet, R. Garcia, R. Haus, J. Helbert, N. I. Ignatiev, P. G. J. Irwin, Y. Langevin, M. A. Lopez-Valverde, D. Luz, L. Marinangeli, V. Orofino, A. V. Rodin, M. C. Roos-Serote, B. Saggin, D. M. Stam, D. Titov, G. Visconti, M. Zambelli, E. Ammannito, A. Barbis, R. Berlin, C. Bettanini, A. Boccaccini, G. Bonnello, M. Bouye, F. Capaccioni, A. Cardesin Moinelo, F. Carraro, G. Cherubini, M. Cosi, M. Dami, M. de Nino, D. Del Vento, M. di Giampietro, A. Donati, O. Dupuis, S. Espinasse, A. Fabbri, A. Fave, I. F. Veltroni, G. Filacchione, K. Garceran, Y. Ghomchi, M. Giustini, B. Gondet, Y. Hello, F. Henry, S. Hofer, G. Huntzinger, J. Kachlicki, R. Knoll, K. Driss, A. Mazzoni, R. Melchiorri, G. Mondello, F. Monti, C. Neumann, F. Nuccilli, J. Parisot, C. Pasqui, S. Perferi, G. Peter, A. Piacentino, C. Pompei, J.-M. Reess, J.-P. Rivet, A. Romano, N. Russ, M. Santoni, A. Scarpelli, A. Semery, A. Soufflot, D. Stefanovitch, E. Suetta, F. Tarchi,

N. Tonetti, F. Tosi, B. Ulmer, South-polar features on Venus similar to those near the north pole, Nature450 (2007) 637–640. 14, 35

F. W. Taylor, D. J. McCleese, D. J. Diner, Polar clearing in the Venus clouds observed from the Pioneer Orbiter, Nature279 (1979) 613–+. 14

S. S. Limaye, J. P. Kossin, C. Rozoff, G. Piccioni, D. V. Titov, W. J. Markiewicz, Vortex circulation on Venus: Dynamical similarities with terrestrial hurricanes, Geophys. Res. Lett.36 (2009) 4204–+. 15

A. D. del Genio, W. B. Rossow, Planetary-scale waves and the cyclic nature of cloud top dynamics on Venus, Journal of Atmospheric Sciences 47 (1990) 293–318. 15

F. W. Taylor, R. Beer, M. T. Chahine, D. J. Diner, L. S. Elson, R. D. Haskins, D. J. McCleese, J. V. Martonchik, P. E. Reichley, S. P. Bradley, J. Delderfield, J. T. Schofield, C. B. Farmer, L. Froidevaux, J. Leung, M. T. Coffey, J. C. Gille, Structure and meteorology of the middle atmosphere of Venus Infrared remote sensing from the Pioneer orbiter, J. Geophys. Res.85 (1980) 7963–8006. 15

R. V. Yelle, D. F. Strobell, E. Lellouch, D. Gautier, The Yelle Titan Atmosphere Engineering Models, in: A. Wilson (Ed.), Huygens: Science, Payload and Mission, Vol. 1177 of ESA Special Publication, 1997, pp. 243–+. 16

M. Fulchignoni, F. Ferri, F. Angrilli, A. J. Ball, A. Bar-Nun, M. A. Barucci, C. Bettanini, G. Bianchini, W. Borucki, G. Colombatti, M. Coradini, A. Coustenis, S. Debei, P. Falkner, G. Fanti, E. Flamini, V. Gaborit, R. Grard, M. Hamelin, A. M. Harri, B. Hathi, I. Jernej, M. R. Leese, A. Lehto, P. F. Lion Stoppato, J. J. López-Moreno, T. Mäkinen, J. A. M. McDonnell, C. P. McKay, G. Molina-Cuberos, F. M. Neubauer, V. Pirronello, R. Rodrigo, B. Saggin, K. Schwingenschuh, A. Seiff, F. Simões, H. Svedhem, T. Tokano, M. C. Towner, R. Trautner, P. Withers, J. C. Zarnecki, In situ measurements of the physical characteristics of Titan's environment, Nature438 (2005) 785–791. 16

E. R. Stofan, C. Elachi, J. I. Lunine, R. D. Lorenz, B. Stiles, K. L. Mitchell, S. Ostro, L. Soderblom, C. Wood, H. Zebker, S. Wall, M. Janssen, R. Kirk, R. Lopes, F. Paganelli, J. Radebaugh, L. Wye, Y. Anderson, M. Allison, R. Boehmer, P. Callahan, P. Encrenaz, E. Flamini, G. Francescetti, Y. Gim, G. Hamilton, S. Hensley, W. T. K. Johnson, K. Kelleher, D. Muhleman, P. Paillou, G. Picardi, F. Posa, L. Roth, R. Seu, S. Shaffer, S. Vetrella, R. West, The lakes of Titan, Nature445 (2007) 61–64. 17

R. H. Brown, L. A. Soderblom, J. M. Soderblom, R. N. Clark, R. Jaumann, J. W. Barnes, C. Sotin, B. Buratti, K. H. Baines, P. D. Nicholson, The identification of liquid ethane in Titan's Ontario Lacus, Nature454 (2008) 607–610. 17

B. A. Ivanov, A. T. Basilevsky, G. Neukum, Atmospheric entry of large meteoroids: implication to Titan, PlanSS45 (1997) 993–1007. 17

A. L. Broadfoot, B. R. Sandel, D. E. Shemansky, J. B. Holberg, G. R. Smith, D. F. Strobel, J. C. McConnell, S. Kumar, D. M. Hunten, S. K. Atreya, T. M. Donahue, H. W. Moos,

J. L. Bertaux, J. E. Blamont, R. B. Pomphrey, S. Linick, Extreme ultraviolet observations from Voyager 1 encounter with Saturn, Science 212 (1981) 206–211. 18

R. Hanel, B. Conrath, F. M. Flasar, V. Kunde, W. Maguire, J. C. Pearl, J. Pirraglia, R. Samuelson, L. Herath, M. Allison, D. P. Cruikshank, D. Gautier, P. J. Gierasch, L. Horn, R. Koppany, C. Ponnamperuma, Infrared observations of the Saturnian system from Voyager 1, Science 212 (1981) 192–200. 18

R. E. Samuelson, R. A. Hanel, V. G. Kunde, W. C. Maguire, Mean molecular weight and hydrogen abundance of Titan's atmosphere, Nature292 (1981) 688–693. 18

G. R. Smith, D. F. Strobel, A. L. Broadfoot, B. R. Sandel, D. E. Shemansky, J. B. Holberg, Titan's upper atmosphere - Composition and temperature from the EUV solar occultation results, J. Geophys. Res.87 (1982) 1351–1359. 18

D. F. Strobel, D. E. Shemansky, EUV emission from Titan's upper atmosphere - Voyager 1 encounter, J. Geophys. Res.87 (1982) 1361–1368. 18

G. F. Lindal, G. E. Wood, H. B. Hotz, D. N. Sweetnam, V. R. Eshleman, G. L. Tyler, The atmosphere of Titan - an analysis of the Voyager 1 radio occultation measurements, Icarus 53 (1983) 348–363. 18, 19, 20, 46, 50

B. L. Lutz, C. de Bergh, T. Owen, Titan - Discovery of carbon monoxide in its atmosphere, Science 220 (1983) 1374–+. 18

M. E. Brown, A. H. Bouchez, C. A. Griffith, Direct detection of variable tropospheric clouds near Titan's south pole, Nature420 (2002) 795–797. 18

F. M. Flasar, R. E. Samuelson, B. J. Conrath, Titan's atmosphere - Temperature and dynamics, Nature292 (1981) 693–698. 19, 21

M. K. Bird, M. Allison, S. W. Asmar, D. H. Atkinson, I. M. Avruch, R. Dutta-Roy, Y. Dzierma, P. Edenhofer, W. M. Folkner, L. I. Gurvits, D. V. Johnston, D. Plettemeier, S. V. Pogrebenko, R. A. Preston, G. L. Tyler, The vertical profile of winds on Titan, Nature438 (2005) 800–802. 21

F. M. Flasar, M. D. Allison, J. I. Lunine, Titan Zonal Wind Model, in: A. Wilson (Ed.), Huygens: Science, Payload and Mission, Vol. 1177 of ESA Special Publication, 1997, pp. 287–+. 21

F. Hourdin, O. Talagrand, R. Sadourny, R. Courtin, D. Gautier, C. P. McKay, Numerical simulation of the general circulation of the atmosphere of Titan., Icarus 117 (1995) 358–374. 22, 24, 25, 50, 51, 55

T. Tokano, F. M. Neubauer, Tidal Winds on Titan Caused by Saturn, Icarus 158 (2002) 499–515. 22

E. Kalnay de Rivas, Further numerical calculations of the circulation of the atmosphere of Venus., Journal of Atmospheric Sciences 32 (1975) 1017–1024. 23

H. G. Mayr, I. Harris, Quasi-axisymmetric circulation and superrotation in planetary atmospheres, Astronomy and Astrophysics121 (1983) 124–136. 23

S. Lebonnois, F. Hourdin, V. Eymet, A. Crespin, R. Fournier, F. Forget, Superrotation of Venus' atmosphere analysed with a full General Circulation Model, in Prep. 24, 56

J. L. Hollingsworth, R. E. Young, G. Schubert, C. Covey, A. S. Grossman, A simple-physics global circulation model for Venus: Sensitivity assessments of atmospheric superrotation, Geophys. Res. Lett.34 (2007) 5202–+. 24

H. F. Parish, G. Schubert, C. C. Covey, A. Grossman, Simulation of Venus Atmosphere Dynamics With an Earth Climate GCM, AGU Fall Meeting Abstracts. 24

K. Ikeda, M. Yamamoto, M. Takahashi, Superrotation of the Venus atmosphere simulated by an Atmospheric General Circulation Model, in: IUGG/IAMAS Meeting, Vol. Perugia, Italy, 2007. 24

V. Eymet, R. Fournier, S. Lebonnois, J.-L. Dufresne, F. Hourdin, M. Bullock, Net-Exchange parameterization of thermal infrared radiative transfer in Venus' atmosphere, in Prep. 24, 39, 40

T. Nakajima, M. Tsukamoto, Y. Tsushima, A. Numaguti, T. Kimura, Modeling of the Radiative Process in an Atmospheric General Circulation Model, Applied Optics39 (2000) 4869–4878. 24

S. Lebonnois, F. Forget, F. Hourdin, Using Terrestrial GCMs to Understand Climate on Venus, Mars and Titan, AGU Fall Meeting Abstracts (2008) B2+. 24

A. D. del Genio, W. Zhou, T. P. Eichler, Equatorial superrotation in a slowly rotating GCM - Implications for Titan and Venus, Icarus 101 (1993) 1–17. 24

C. P. McKay, J. B. Pollack, R. Courtin, The thermal structure of Titan's atmosphere, Icarus 80 (1989) 23–53. 25, 46

P. Rannou, S. Lebonnois, F. Hourdin, D. Luz, Titan atmosphere database, Advances in Space Research 36 (2005) 2194–2198. 25

T. Tokano, F. M. Neubauer, M. Laube, C. P. McKay, Seasonal variation of Titans atmospheric structuresimulated by a general circulation model, PlanSS47 (1999) 493–520. 25

C. E. Newman, M. I. Richardson, C. Lee, A. D. Toigo, S. P. Ewald, The TitanWRF Model at the end of the Cassini Prime Mission., AGU Fall Meeting Abstracts (2008) A2+. 25

M. J. P. Cullen, T. Davies, M. H. Mawson, Conservative finite diferences schemes for a unified forecast/climate model. , Unified Model Documentation Paper No. 10. Meteorological Office, UK. 27

L. Colin, Basic facts about Venus, 1983, pp. 10–26. 27

A. Arakawa, V. R. Lamb, A potential enstrophy and energy conserving scheme for the shallow water equations, Monthly Weather Review 109 (1981) 18–36. 27

A. Seiff, Thermal structure of the atmosphere of Venus, 1983, pp. 215–279. 30

M. G. Tomasko, L. R. Doose, P. H. Smith, The absorption of solar energy and the heating rate in the atmosphere of Venus, Advances in Space Research 5 (1985) 71–79. 30

P. Chen, J. R. Holton, R. Swinbank, A quasi-permeable barrier in the equatorial lower stratosphere, Geophys. Res. Lett.22 (1995) 259–262. 31

E. Shuckburgh, W. Norton, A. Iwi, P. Haynes, Influence of the quasi-biennial oscillation on isentropic transport and mixing in the tropics and subtropics, J. Geophys. Res.106 (2001) 14327–14338. 31

P. Chen, The permeability of the Antarctic vortex edge, J. Geophys. Res.99 (1994) 20563–20572. 31

D. V. Titov, F. W. Taylor, H. Svedhem, N. I. Ignatiev, W. J. Markiewicz, G. Piccioni, P. Drossart, Atmospheric structure and dynamics as the cause of ultraviolet markings in the clouds of Venus, Nature456 (2008) 620–623. 31

W. J. Markiewicz, D. V. Titov, S. S. Limaye, H. U. Keller, N. Ignatiev, R. Jaumann, N. Thomas, H. Michalik, R. Moissl, P. Russo, Morphology and dynamics of the upper cloud layer of Venus, Nature450 (2007) 633–636. 31

M. E. McIntyre, W. A. Norton, Dissipative wave-mean interactions and the transport of vorticity or potential vorticity, Journal of Fluid Mechanics 212 (1990) 403–435. 31

P. Haynes, E. Shuckburgh, Effective diffusivity as a diagnostic of atmospheric transport 1. Stratosphere, J. Geophys. Res.105 (2000) 22777–22794. 33

P. Haynes, E. Shuckburgh, Effective diffusivity as a diagnostic of atmospheric transport 2. Troposphere and lower stratosphere, J. Geophys. Res.105 (2000) 22795–22810. 33

N. Nakamura, Two-Dimensional Mixing, Edge Formation, and Permeability Diagnosed in an Area Coordinate., Journal of Atmospheric Sciences 53 (1996) 1524–1537. 33

A. Piccialli, D. V. Titov, D. Grassi, I. Khatuntsev, P. Drossart, G. Piccioni, A. Migliorini, Cyclostrophic winds from the Visible and Infrared Thermal Imaging Spectrometer temperature sounding: A preliminary analysis, Journal of Geophysical Research (Planets) 113 (E12) (2008) 0–+. 34, 35

J.-L. Dufresne, R. Fournier, C. Hourdin, F. Hourdin, Net Exchange Reformulation of Radiative Transfer in the CO_2 15-μm Band on Mars., Journal of Atmospheric Sciences 62 (2005) 3303–3319. 39, 40

D. Crisp, Radiative forcing of the Venus mesosphere. I - Solar fluxes and heating rates, Icarus 67 (1986) 484–514. 39

W. J. Ingram, S. Woodward, J. Edwards, Radiation. , Unified Model Documentation Paper No. 23. Meteorological Office, UK. Version 4.0. 39

F. Forget, F. Hourdin, R. Fournier, C. Hourdin, O. Talagrand, M. Collins, S. R. Lewis, P. L. Read, J.-P. Huot, Improved general circulation models of the Martian atmosphere from the surface to above 80 km, J. Geophys. Res.104 (1999) 24155–24176. 39, 56

J. S. A. Green, Division of radiative streams into internal transfer and cooling to space, Quarterly Journal of the Royal Meteorological Society 93 (1967) 371–372. 40

S. Lebonnois, F. Hourdin, V. Eymet, R. Fournier, J.-L. Dufresne, A new Venus General Circulation Model, in the context of the Venus-Express mission, in: Bulletin of the American Astronomical Society, Vol. 37 of Bulletin of the American Astronomical Society, 2005, pp. 742–+. 40

V. Eymet, R. Fournier, S. Blanco, J. L. Dufresne, A boundary-based net-exchange Monte Carlo method for absorbing and scattering thick media, Journal of Quantitative Spectroscopy and Radiative Transfer 91 (2005) 27–46. 41

V. Eymet, KARINE: a tool for infrared radiative transfer analysis in planetary atmospheres, Note internr, Laboratire d'Energétique, France. 41

L. V. Zasova, N. Ignatiev, I. Khatuntsev, V. Linkin, Structure of the Venus atmosphere, PlanSS55 (2007) 1712–1728. 41

L. Zuchowski, Modelling Jupiter's jet scale, meridional circulations, cloud bands and moist convective storms., Ph.D. thesis, PhD Thesis, Oxford University (2009). 43

A. Seiff, J. T. Schofield, A. J. Kliore, F. W. Taylor, S. S. Limaye, Models of the structure of the atmosphere of Venus from the surface to 100 kilometers altitude, Advances in Space Research 5 (1985) 3–58. 44, 56

C. P. McKay, J. B. Pollack, R. Courtin, The thermal structure of Titan's atmosphere, Icarus 80 (1989) 23–53. 50

P. G. J. Irwin, N. A. Teanby, R. de Kok, L. N. Fletcher, C. J. A. Howett, C. C. C. Tsang, C. F. Wilson, S. B. Calcutt, C. A. Nixon, P. D. Parrish, The NEMESIS planetary atmosphere radiative transfer and retrieval tool, Journal of Quantitative Spectroscopy and Radiative Transfer 109 (2008) 1136–1150. 55, 56

N. A. Teanby, R. de Kok, P. G. J. Irwin, S. Osprey, S. Vinatier, P. J. Gierasch, P. L. Read, F. M. Flasar, B. J. Conrath, R. K. Achterberg, B. Bézard, C. A. Nixon, S. B. Calcutt, Titan's winter polar vortex structure revealed by chemical tracers, Journal of Geophysical Research (Planets) 113 (12) (2008) 12003–+. 57

D. G. Andrews, J. R. Holton, C. B. Leovy, Middle atmosphere dynamics., 1987. 60